UNIVERSITÀ DEGLI STUDI DI MILANO

Ph.D. course in **Molecular and Cellular Biology**
XXXVIII cycle

Department of Biosciences

The lysosomal amyloid aggregation of β_2-microglobulin promotes multiple myeloma progression: a molecular focus on this pro-cancer mechanism

Giulia Rizzi
R13768 ORCID n°: 0000-0002-0635-4729

Scientific tutor: **Stefano Ricagno**

PhD coordinator: **Stefano Ricagno**

A.A. 2024/2025

RIASSUNTO

Il mantenimento della struttura nativa è cruciale per l'attività biologica delle proteine. Pertanto, le cellule hanno evoluto diversi meccanismi di controllo per preservarla. Quando questi meccanismi non funzionano correttamente, la conformazione delle proteine può andare incontro a destabilizzazione e parziale unfolding. Questi eventi sono alla base di una specifica classe di patologie chiamate malattie da misfolding proteico, caratterizzate dalla formazione di aggregati che, accumulandosi all'interno di tessuti o organi, ne compromettono la funzionalità. In questo contesto, β2-microglobulina (β2m) è stata ampiamente studiata poiché la sua aggregazione sottoforma di fibrille amiloidi porta all'insorgenza di una specifica amiloidosi associata a dialisi. Inoltre, la concentrazione sierica di β2m è usata come fattore prognostico per diverse malattie ematologiche, tra cui il mieloma multiplo (MM). Studi recenti hanno dimostrato che l'accumulo e l'aggregazione di β2m all'interno dei lisosomi dei macrofagi associati al tumore contribuisce attivamente alla progressione del MM. L'accumulo di queste fibrille provoca la rottura dei lisosomi e la conseguente attivazione dell'inflammasoma NLRP3, un complesso proteico che favorisce l'infiammazione e la proliferazione delle cellule tumorali. Questa tesi indaga la relazione tra la propensione all'aggregazione di β2m in condizioni lisosomiali e la conseguente infiammazione. La proteina wild-type (wt) e quattro sue varianti, D76N, ΔN6, D59P e W60G, sono state espresse, purificate e caratterizzate in termini di stabilità al pH e alla temperatura, flessibilità e propensione all'aggregazione a pH fisiologico e lisosomiale. Parallelamente, sono stati condotti studi cellulari su macrofagi differenziati a partire da cellule THP-1 per monitorare l'effetto indotto dalla fagocitosi della proteina sull'integrità lisosomiale, l'attivazione dell'inflammasoma e il rilascio di citochine pro-infiammatorie. Questi esperimenti hanno rivelato che la stabilità di ΔN6 e D59P è fortemente compromessa dal pH lisosomiale, a differenza di W60G, la cui struttura nativa non è affetta dalla riduzione del pH. B2m wt e D76N hanno dimostrato una stabilità intermedia. Inoltre, dalle analisi cellulari è stato osservato che le varianti più prone all'aggregazione inducono una risposta infiammatoria più rapida. Complessivamente, questi risultati stabiliscono una connessione tra la stabilità strutturale di β2m e la sua attività proinfiammatoria, supportando l'ipotesi che β2m non sia soltanto un biomarcatore, ma che svolga anche un ruolo attivo nella progressione del MM. In aggiunta, sono stati sviluppati due progetti paralleli: il primo ha portato alla caratterizzazione di molecole per stabilizzare la struttura di β2m in condizioni lisosomiali; il

secondo, ha permesso di studiate tramite mutagenesi sito-diretta una deaminasi (RidA) per caratterizzarne l'eccezionale stabilità e attività enzimatica.

ABSTRACT

Maintenance of native folding is crucial for ensuring protein biological activity. Despite cells have evolved several control mechanisms to preserve folding, when they fail, proteins undergo destabilization or partial unfolding, events that favor the onset of protein misfolding diseases. These conditions are characterized by formation of protein aggregates, which impair tissues and organ functionalities. A widely studied example is β_2-microglobulin (β_2m), whose aggregation into amyloid fibrils underlies dialysis-related amyloidosis. Beyond this role, β_2m also serves as prognostic factor for several hematological malignancies, including multiple myeloma (MM). Recent studies demonstrated that β_2m actively contributes to MM pathogenesis by aggregating inside the lysosomes of tumor-associated macrophages. The resulting lysosomal damage induces NLRP3 inflammasome activation which sustain inflammation and malignant plasma cell proliferation. This thesis investigates the link between β_2m fold stability and aggregation propensity under lysosomal-like conditions, and the resulting inflammatory response in macrophage-like cells. Wild-type and four β_2m variants, namely D76N, ΔN6, D59P, and W60G were expressed, purified, and biophysically characterized in terms of pH and temperature stability, flexibility and aggregation propensity under physiological and lysosomal-like pH. In parallel, cellular studies were performed on THP-1-derived macrophages to monitor the effect of β_2m uptake on lysosomal integrity, inflammasome activation, cytokine release, and cell viability. The biophysical analysis revealed three stability groups: ΔN6 and D59P, strongly destabilized by lysosomal pH and highly aggregation-prone; wt and D76N, with intermediate stability; and W60G, remarkably resistant to pH destabilization and aggregation. In cells, aggregation-prone variants formed large intracellular foci that increased in number and size over time. Furthermore, a prolonged NLRP3 and caspase-1 activation, as well as elevated IL-1β release was detected. In contrast, W60G, by remaining stable under lysosomal conditions, did not lead to aggregate formation, and neither to inflammasome activation and inflammatory cytokine release. Taken together, these results establish a direct link between β_2m structural stability and its capacity to modulate macrophage-driven inflammation, supporting the evidence that β_2m is not only a biomarker but also an active pathogenic factor in MM.

Additionally, two distinct side projects were developed. The first aiming at the characterization of affinity molecules designed to stabilize β_2m fold under lysosomal-like conditions; in the second a site-directed mutagenesis was applied on reactive intermediate deaminase to characterize the remarkable stability and enzymatic potential of this enzyme.

TABLE OF CONTENT

LIST OF ABBREVIATIONS

ERAD: Endoplasmic reticulum-associated degradation

ATP: Adenosine triphosphate

Hsp70: Heat-shock protein 70

ER: Endoplasmic reticulum

CFTR: Cystic fibrosis transmembrane conductance regulator

AD: Alzheimer's disease

PD: Parkinson's disease

AL amyloidosis: Light chain amyloidosis

ThT: Thioflavin T

ThS: Thioflavin S

A-beta: Amyloid beta

β_2m: Beta$_2$-microglobulin

α-syn: α-
synuclein

APRs: Aggregation-prone regions

Val or V: Valine

Leu: Leucine

Ile: Isoleucine

ROS: Reactive oxygen species

MHC-I: Major histocompatibility complex-I

Cys or C: Cysteine

DRA: Dialysis-related amyloidosis

NLRP3: NOD-, LRR- and pyrin domain-containing protein

Asp or D: Aspartate

Asn or N: Asparagine

Pro or P: Proline

Trp or W: Tryptophan

Gly or G: Glycine

Phe or F: Phenylalanine

MM: Multiple myeloma

CPCs: Circulating plasma cells

TAMs: Tumor-associated macrophages

ASC: Apoptosis-associated speck-like protein containing a CARD
PYD: PYRIN domain

LLR: Leucine-rich repeat

PAMPs: Pathogen-associated molecular patterns

DAMPs: Damage-associated molecular patterns

TLRs: Toll-like receptors

IL: Interleukin

TNF: Tumor necrosis factor

NF-κB: Nuclear factor κB

wt: Wild-type

CD: Circular dichroism

T_m: Melting temperature

pH_m: pH melting

SDS-PAGE: Sodium dodecyl sulphate polyacrylamide gel electrophoresis

TEM: Transmission electron microscopy

PMA: phorbol-12-myristate-13-acetate

LPS: Lipopolysaccharide

MTT: 3-(4,5-dimethylthiazol-2-yl)-2,5-diphenyltetrazolium bromide

SD. Standard deviation

AF-488: Alexa fluor 488

LAMP1: Lysosomal-associated membrane protein 1

GAPDH: Glyceraldehyde-3-phosphate dehydrogenase

Wb: Western blot

ELISA: Enzyme-linked immunosorbent assay

GSDMD: Gasdermin D

RT: Room temperature

ΔH: Molar reaction enthalpy

K_D: Dissociation constant

2AA: 2-aminoacrylate

Lys: Lysine

Glu: Glutamate

Ala: Alanine

Tyr: Tyrosine

1. INTRODUCTION

1.1. Protein folding and misfolding

The ability of proteins to exert their biological activity is strictly connected to their three-dimensional organization. Under controlled physiological conditions protein folding can occur spontaneously; indeed, most of the information required for protein native assembly lies in its amino acid sequence[1,2]. However, achieving the correct folding becomes considerably more challenging for proteins with complex or multidomain assemblies, which constitute most of the proteome. In these cases, the number of theoretically accessible conformation for the proteins is incredibly large. Nonetheless, these proteins still reach their functional structures efficiently by diffusing along an energy landscape encoded by their amino acid sequence[3]. This landscape limits the conformational space sampled by the polypeptide and guides the chain toward its lowest energy level[4]. In this framework, folding specificity arises from sequence heterogeneity, as the distinct energetic contributions of each residue favor specific structural rearrangements over others[5]. Consequently, even subtle changes in the protein sequence, such as point mutations, can reshape the energy landscape and lead to alternative native conformations, characterized by a specific energy level. Additionally, in physiological conditions, proteins do not exist as single static structures but instead populate an ensemble of conformational states separated by kinetic barriers and modulated by intrinsic dynamics, interaction partners, and thermal fluctuations[6].

The folding process becomes even trickier moving from *in vitro* to *in vivo* systems, due to the high complexity of the cellular environment. Here proteins may undergo multiple rounds of unfolding and refolding to translocate between different cellular compartments[7], fold upon binding to other proteins[8], experience macromolecular crowding[9] and abiotic stresses[10]. To grant protein correct folding and prevent the detrimental effects induced by their non-functional transition and aggregation, the cell has evolved several control systems. In this context, chaperones and protein degradation mechanisms, namely endoplasmic reticulum-associated degradation (ERAD)[11,12] (Figure 1) and autophagy[13] (Figure 2), play a crucial role.

1.1.1 Cellular systems involved in protein folding

Molecular chaperones are proteins that recognize and interact with exposed hydrophobic residues and unstructured regions of the proteins. This interaction facilitates efficient intramolecular assembly and prevents intermolecular aggregation[14–16]. Chaperones can work at various stages of the folding process, engaging interactions with both nascent polypeptide chains and fully synthesized proteins[5]. The activity of these enzymes can be both ATP-dependent, as Hsp70, or -independent, as SurA[15]. In the former case, ATP is required to allow the catalytic cycle, as well as the regulation of allosteric changes in the chaperone, or the binding and release of the substrate[17]. In the latter case, the binding of chaperone alone to the substrate allows the shielding of the exposed hydrophobic regions, which are potential drivers of aggregation[18].

Protein degradation systems come into play upon protein irreversible misfolding to avoid the intracellular accumulation of aggregates that can impair cell homeostasis and eventually result in cell toxicity[11]. The ERAD pathway allows proteasomal degradation of damaged proteins after polyubiquitination. This process is carried out by the concerted activity of three enzymes: E1, that activates the ubiquitin, E2, the ubiquitin-conjugating enzyme and E3 ligase, that provides substrate specificity through the recognition of specific peptide motifs[19,20]. During protein degradation, ubiquitination occurs repeatedly, resulting in the formation of diverse ubiquitin chains that target substrates to the proteasome[20,21]. At the proteasome, ubiquitin tags are recognized by specific receptors, initiating the degradation at the unstructured region of the substrate. The protein is then completely unfolded and, through ATP hydrolysis, translocated to the central catalytic cavity of the proteasome, where it undergoes sequential proteolysis[22] (Figure 1).

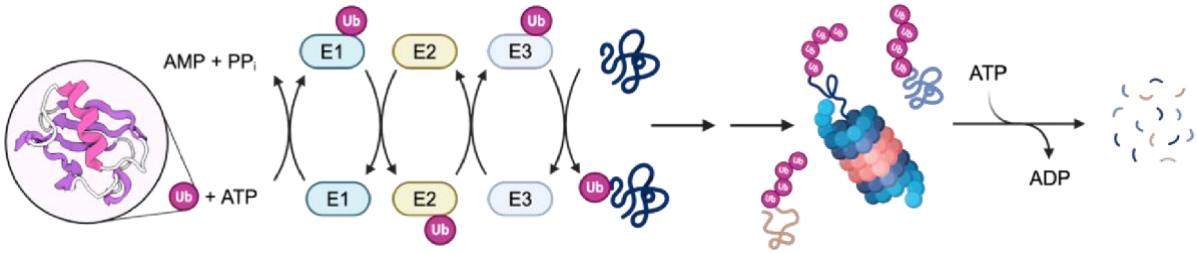

Figure 1: **Endoplasmic reticulum-associated degradation pathway.** The misfolded protein is ubiquitinated by the subsequent activity of E1, E2 and E3 enzymes. The ubiquitin tag allows the protein to be recognized by the proteasome that, through ATP hydrolysis, degrades it. Created in https://BioRender.com

However, bulk protein aggregates can clog the proteasome channel and therefore block the degradation machinery. In these cases, autophagy is stimulated[13,23]. There are three main forms of autophagy: microautophagy, which facilitates the disposal of damaged organelles, macroautophagy and chaperone-mediated autophagy, which instead are involved in protein degradation. Macroautophagy is the preferred cellular mechanism for the degradation of whole protein aggregates through the formation of autophagosome, a double-membrane structure that eventually fuses with the lysosome forming the autolysosome[24]. The low pH within the autolysosome facilitates conformational changes in the aggregates, making them susceptible to degradation by lysosomal proteases[25] (Figure 2).

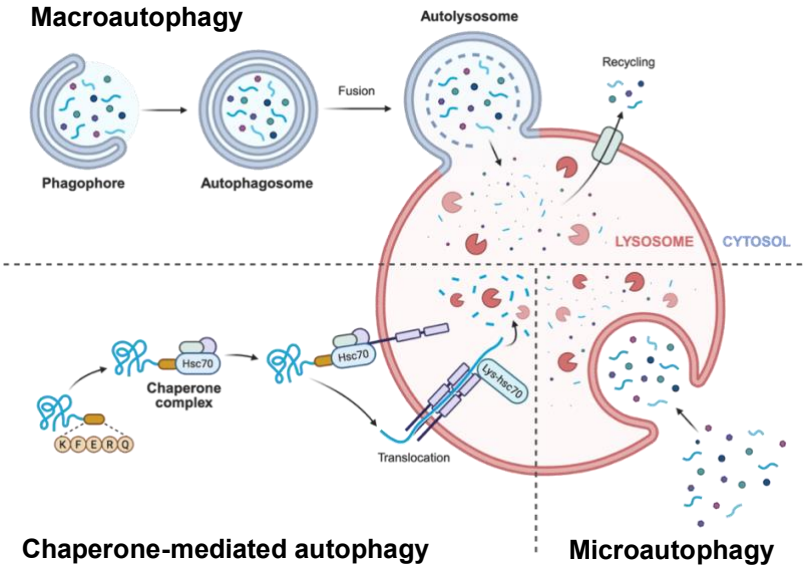

Figure 2: **The main mechanisms of autophagy**. Macroautophagy and chaperone-mediated autophagy are the preferred mechanisms for degradation of misfolded proteins. Macroautophagy involves the formation of a double membrane structure, the autophagosome, that, by fusion with the lysosome, allows the degradation and recycling of the internalized components. Microautophagy allows the direct degradation of damaged organelles, without formation of the autophagosome. Created in https://BioRender.com

If these quality controls fail, whether due to mutation, aging, or chronic endoplasmic reticulum (ER) stress (as during excessive insulin production by β-cells in diabetes), proteins may become unable to adopt or maintain their native conformation. This fosters the onset of pathologies collectively known as misfolding diseases[6,14,26].

1.1.2 Protein misfolding diseases

Protein misfolding diseases (also known as conformational diseases) are a broad and heterogeneous class of pathologies characterized by altered protein folding stability[6]. They can be triggered by several factors, such as the presence of mutations, post-translational modifications (as hyperphosphorylation), cellular stress (changes in temperature or pH) or failure in protein control mechanisms[6]. According to the effects triggered by the alteration in the protein assembly, misfolding diseases can be broadly classified into two categories: those caused by the loss of the specific physiological function encoded by the protein, and those driven by gain of toxic function.

In the first case, the nonfunctional misfolded protein is recognized by the cellular control system and rapidly degraded. Therefore, the pathological state results from the lack of the native protein and the consequent alteration of the cellular or metabolic activity involving the protein itself. An example of loss-of-function misfolding disease is cystic fibrosis, a genetic condition caused by mutations in the gene encoding for cystic fibrosis transmembrane conductance regulator (CFTR), an ion channel responsible for the extracellular transportation of chloride ions and water, which allows the maintenance of the fluidity of mucus secretions[27].

However, the typical scenario in protein misfolding diseases is represented by the gain of toxic function, in which the establishment of aberrant intermolecular interactions promotes the formation of insoluble aggregates. Frequently, these aggregates fail to be efficiently eliminated by protein quality control systems and deposit inside cells, tissues and organs, inducing dysfunction[28]. A critical risk factor in this class of pathologies is represented by age. Indeed, during aging, cells accumulate endogenous and exogenous stresses that impair the quality control network, preventing proteostasis maintenance and, therefore, the proper dismantling of misfolded and aggregated proteins. This scenario is typical of neurodegenerative disorders, such as Alzheimer's (AD) and Parkinson's diseases (PD), in which the interplay of genomic instability, telomere shortening, epigenetic alterations and loss of proteostasis contribute to the degenerative process[29].

Conformational diseases can also be classified according to their localization. In localized pathologies, as in the case of AD and PD, the protein agglomerates accumulate in a single organ[29]. Differently, in systemic conditions the deposition of the aggregates is spread to multiple organs simultaneously, as in the case of light-chain amyloidosis (AL amyloidosis),

in which clusters of aggregated light chains are found inside kidneys, heart, spleen and liver[30].

In conclusion, protein misfolding diseases are a highly heterogenous and complex group of disorders, characterized by remarkable variability in their clinical manifestation. This heterogenicity poses major challenges in the development of effective treatments, and consequently, most of these pathologies remains uncurable[6].

1.1.3 Structural features of amyloid fibrils

Most of the protein aggregates associated with protein misfolding diseases consists of amyloid fibrils. These are elongated unbranched filaments characterized by a cross-β conformation that confers the fibrils remarkable stability and resistance to proteolytic cleavage[31]. From the structural point of view, amyloid fibrils have a hierarchical organization. They are typically constituted by one or more protofilaments, stacked one another through sidechains interactions with a width ranging from 7 to 13 nm[6]. Each protofilament consists of monomeric subunits constituted by stacked β-strands linked one another through hydrogen bonds running parallel to the protofilament axis.

There are different dyes that can be used to detect the presence and monitor the formation of fibrils *in vitro*. Congo Red is a direct diazo dye which emits green birefringence under-cross polarized light typically used to stain amyloids in tissue sections[32]. Thioflavin-T (ThT) is a thiazole compound, which displays enhanced fluorescent signal upon binding to cross-β structure, and a red shift of its emission spectrum[33]. Thioflavin-S (ThS) is a mixture of compounds which emit a yellow-green fluorescence when bound to amyloids.

Despite the variability in the native secondary and tertiary structure of the precursor proteins[34], the overall architecture of the deriving fibrils is highly similar. The main feature defining amyloid fibrils is their cross-β structure, consisting in several sheets twisting around a central axis, which are stabilized by an array of hydrophobic and polar interactions running along the fibril backbone[35]. The subtle changes that can be observed in term of shape, size and fibrillation kinetics are mainly dictated by the protein sequence[36]. Concurrently, amyloid fibers exhibit high heterogenicity among them, with the same precursor protein capable of forming different polymorphisms with distinct structure and biological properties[6,36]. Such heterogenicity typical of the amyloid fibrils represents a difference from the native protein structure. Indeed, while a given polypeptide chain always folds into a unique three-dimensional conformation, defined by a distinct pattern of side-chain interactions, amyloid

fibril formation is different: the same sequence can adopt multiple conformationally stable states, each characterized by different networks of inter-residue interactions[37]. A remarkable example of such amyloid fibril heterogenicity is represented by amyloid β(1-40) fragment (A-beta), for which numerous polymorphisms have been described, differing in the number of protofilaments, their relative orientation, and conformation of the constituent peptides (Figure 3)[37,38].

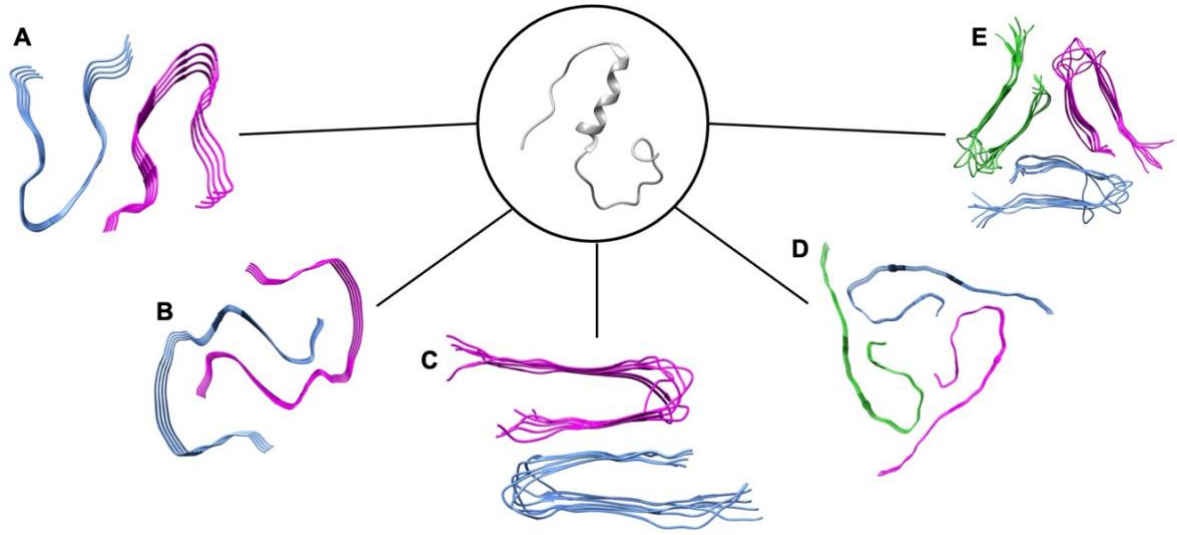

Figure 3: **Amyloid-β(1-40) can assemble into different polymorphisms upon fibril formation**. A-beta fibrils are highly polymorphic, containing different numbers protofilaments. (**A**-**B**) Polymorphic fibrils found in the brain tissue of an AD patient; (**C**-**D**) fibrils grown *in vitro* with striated and twisted morphology; (**D**) fibrils extracted from brain tissue of AD patient (PDB ID A-beta: 2LFM; A: 8EZD; B: 8EZE; C: 2MLN; D: 2LMP; E: 2M4J). (**D**-**E**). Molecular graphics performed with UCSF Chimera.

1.1.4 Molecular mechanisms of amyloid fibril formation

Protein aggregation is a complex and heterogeneous process that involves several transition steps, regulated by a network of thermodynamic equilibria and kinetic barriers, strongly influenced by the protein amino acidic sequence[39]. In their native state, amyloidogenic proteins may adopt either a compact, globular form, as in the case of lysozyme, transthyretin or β_2-microglobulin (β_2m), or a predominantly disordered, random-coil conformation, as observed for A-beta, α-synuclein (α-syn) or tau. Upon structural destabilization, that can be triggered by proteolytic degradation, cellular stress or defects in the quality control

machinery, the native globular structure of the protein starts to unfold[40,41]. The accumulation of partially folded species promotes a further destabilization of the soluble protein, accelerating its aggregation[42]. Differently, for physiologically unstructured proteins the aggregation process mainly consists in the self-assembly of the different conformers present in solution[40–42]. In both the cases, destabilization drives the protein population towards unstable and partially ordered conformations. These intermediates are highly prone to self-assemble into fibrils upon exposure of short amino acid stretches called aggregation prone regions (APRs)[43]. The comparative analysis of APRs from different amyloidogenic proteins revealed several shared features in their amino acid composition, including preference for β-branched hydrophobic residues (such as Val, Leu and Ile), strong β-sheet propensity and low net charge[44]. These sequences are normally buried inside the hydrophobic core of the native protein and, when they get exposed to the aqueous environment, they readily interact each other, generating the so called cross-β steric zipper motif, the basic structural unit of the amyloid fibrils[45]. This motif is constituted by the intersection of two βsheets, that form a tightly packed interface stabilized by complementary sidechain interactions.

From a mechanistic point of view, amyloid fibril formation is a nucleation-dependent process, consisting of three subsequent steps: nucleation (lag phase), elongation (exponential phase), and plateau (stationary phase)[46–48]. The typical aggregation kinetics outlines a sigmoidal curve, whose shape is predominantly determined by the rates of nucleation and elongation steps[47,49]. The primary nucleation phase corresponds to the time required for monomeric proteins to assemble into active nuclei. This conversion is thermodynamically unfavored and therefore represents the rate-limiting step of the aggregation reaction[49]. During the elongation phase, the generated nuclei act as seeding intermediates that recruit additional monomeric subunits, giving rise to prefibrillar structures, that rapidly grow to form protofibrils[46,49]. Finally, the plateau phase consists in the assembly of protofibrils into mature amyloid fibrils, which can display different morphologies and polymorphic states[46]. Additionally, fibrils can further grow through secondary nucleation events, in which the already formed fibrils accelerate the formation of novel aggregates from free protein monomers[50] (Figure 4).

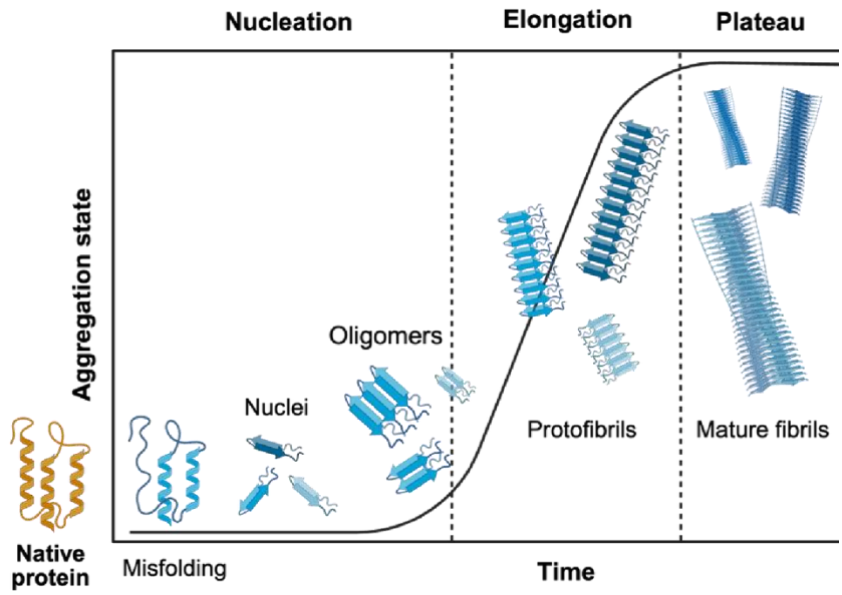

Figure 4: **Protein aggregation kinetics**. The conversion of a soluble protein into highly ordered fibrillar structure requires the partial unfolding of the native state and the formation of reactive nuclei that, by stepwise assembly, lead to formation of mature fibrils. Created in https://BioRender.com

In conclusion, protein aggregation is a complex and layered process, influenced by the interaction of the protein intrinsic characteristics with the cellular environment. However, the increasing knowledge collected on the fundamental molecular mechanism regulating amyloid aggregation is fostering the development of more reliable methods for early diagnosis of protein misfolding disease and for the rational design of effective therapeutic approaches to combat them.

1.1.5 Toxicity of amyloid aggregates

A critical aspect in the study of amyloid-related diseases lies in identifying the molecular species responsible for toxicity. The two most investigated species are oligomers and mature fibrils.

Originally, amyloid fibrils were considered the primarily mediators of cytotoxicity, as suggested by the amyloid hypothesis proposed to explain the pathogenic role played by amyloid plaques in AD[51]. Nonetheless, more recent evidence has increasingly implicated prefibrillar species, particularly oligomers, as the main contributors to toxicity[52]. In the context of AD for instance, A-beta oligomers have been shown to markedly impair cognitive functions and suppress synaptic plasticity[53,54].

Oligomers are soluble prefibrillar structures formed through the self-association of partially unfolded monomeric proteins. Their toxicity has been linked to both their size and the extent of the exposed hydrophobic surface. In particular, smaller oligomers are generally considered as more toxic, as their higher diffusion coefficient allows them to move more rapidly, thereby increasing the likelihood to form aberrant interactions[55]. Additionally, oligomers with less-packed hydrophobic cores tend to be more toxic, since their exposed hydrophobic sequences can penetrate cell membrane and cause perturbation of cell homeostasis.

However, even mature fibril accumulation is implicated in several pathological conditions. Indeed, the extracellular deposition of amyloids can severely compromise organ integrity and function, as observed in some forms of systemic amyloidosis. In dialysis-related amyloidosis the β_2m fibril accumulation leads to osteoarticular pain and, eventually, severe visceral lesions[56]. Fibrils can also promote the generation of new toxic oligomers through secondary nucleation, increasing the number of potentially harmful species[57]. Furthermore, growing evidence indicates that amyloid fibrils can be internalized by cells through the endo-lysosomal system and induce damage to multiple organelles, including endosomes[58], the ER [59] and mitochondria[60].

Several mechanisms have been proposed to explain the toxicity of both oligomers and fibrils, with membrane permeabilization representing the primary one[61]. Numerous studies indicate that protein aggregates can interact with membrane lipids to form transmembrane pore-like structures[62–64] or dissolve membranes in a detergent-like manner[65]. Such pores may form on various cellular membranes, including the smooth ER, the major calcium reservoir of the cell, leading to abnormal release of calcium ions (Ca^{2+}) into the cytoplasm. The subsequent efflux of calcium to the extracellular space, caused by ion channel formation or by increased cell membrane conductance due to lipid bilayer thinning, further exacerbates the unbalance in calcium homeostasis[66]. In addition, ER is also essential for protein and lipid synthesis, folding and transport. Stress conditions induced by the accumulation of aggregates, as reported for α-syn, may compromise the protein folding capacity of ER, further fueling a positive-feedback loop of protein misfolding and cellular dysfunction[67]. Membrane permeabilization and dysregulation in calcium intracellular concentration can trigger several downstream events, including aberrant transmembrane signaling, impairment of mitochondrial function, production of reactive oxygen species (ROS) and ultimately the activation of the apoptotic pathway[68]. Finally, the aggregate accumulation can impair lysosome function. Protein aggregates may directly damage lysosomal membrane, as

observed for A-beta, which compromise autolysosome integrity, causing hydrolase leakage and broad cellular dysfunction[69]. Alternatively, aggregates can interfere with lysosomal gene expression, indirectly reducing degradation capacity, as demonstrated by the inhibition of IST1 expression upon abnormal tau accumulation[70].

In conclusion, both oligomers and fibrils can exert toxicity leading to cellular and organ dysfunction. The design of effective therapeutic strategies remains challenging due to the complexity of the mechanisms regulating the aggregation process and the cellular response upon accumulation of the different molecular species.

1.2 Beta$_2$-microglobulin

Beta$_2$-microglobulin (β_2m) is a 11,900 Da protein present on the membrane of all nucleated cells and in most biological fluids[71,72]. It constitutes the light chain of Major Histocompatibility Complex of Class I (MHC-I)[73], and is present in other MHC-I structurally related proteins like the neonatal Fc receptor[74], the cluster of differentiation 1[75] and the human hemochromatosis protein[76]. Although β_2m does not have catalytic activity, it possesses structural role, allowing the intracellular formation of these complexes, their transport to the membrane, and stabilization upon exposure on the cell surface, establishing non-covalent interactions with the heavy chains[77]. All these features underline the crucial contribution that β_2m plays in proper immune system functioning.

After the release from MHC-I, β_2m enters the bloodstream and reaches the kidneys where it is cleared through glomerular filtration[71,78]. An increased concentration of β_2m in the serum often correlates with pathological onsets due to elevated cellular turnover or impaired kidney function[79]. From the structural point of view, β_2m folds into a β-sandwich structure, constituted by 7 β-strands organized into 2 β-sheets connected by a disulphide bond involving Cys25 on B strand and Cys80 on F strand (Figure 5).

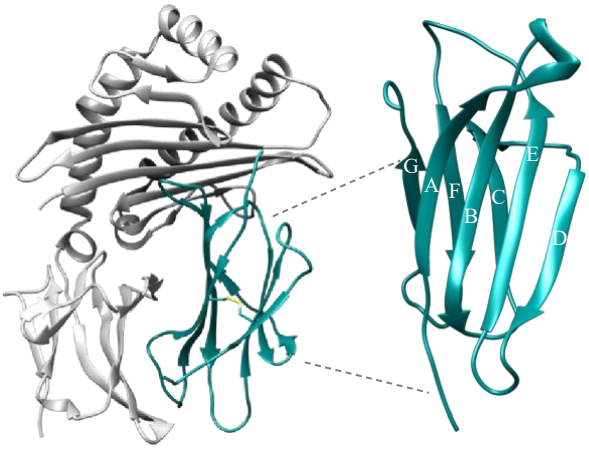

Figure 5: **MHC-I complex** (PDB ID: 4L29). The interaction between the heavy chain (in light grey) and β_2m (in cyan) is granted by the formation of non-covalent interactions. B_2m possesses a β-sandwich structure, constituted by 2 β-sheets of 3 and 4 β-strands each connected by a disulphide bridge establishing between Cys25 and Cys80 (PDB ID: 5CS7).
Molecular graphics performed with UCSF Chimera.

1.2.1 B_2m in pathological conditions

Soluble β_2m is widely present in body fluids, including cerebrospinal fluid, urine and serum. In healthy individuals the β_2m levels in the blood remain relatively stable (between 1.5 – 3 mg/L), with a half-life spanning from 2 to 5 h. An increasing number of studies have highlighted the involvement of β_2m in a wide range of pathological conditions including amyloidosis[80–82], age-dependent neurological disorders[83,84], chronic autoimmune diseases[85–87] and hematological cancers[88,89]. In most of these diseases β_2m is primarily used as biomarker to stage the pathology severity or the patient's prognosis[83–87]. Additionally, in lymphocytic leukemia[90], non-Hodgkin lymphoma[91] and multiple myeloma[88] serum concentration of β_2m was found to strictly correlate with the tumor grade. Although very different from each other, all these conditions share severe dysregulation of the immune system and, particularly in the case of cancer, an elevated cellular turnover, features that significantly contribute to increase the concentration of free β_2m in the bloodstream.
Moreover, β_2m has been extensively studied because of its ability to aggregate into amyloid fibrils, a feature associated with the onset of two distinct forms of amyloidosis: dialysis-related amyloidosis (DRA)[80,81], a iatrogenic condition caused by the aggregation of wild-

type β2m (wt β2m), and hereditary systemic amyloidosis, caused by the aggregation of the genetic β2m variant D76N[82].

More recently, a novel biological role has been described for β2m in the context of multiple myeloma, where the formation of β2m aggregates within tumor-associated macrophages induces lysosomal stress and subsequently triggers a strong NLRP3 (NOD-, LRR- and pyrin domain-containing protein 3)-mediated inflammatory response[92].

1.2.1.1 B2m-related amyloidosis

The first evidence about β2m amyloid behavior was collected in the 1980s. Large deposits of insoluble protein fibrils were found inside the soft tissues, joints and bones of patients undergoing long-term hemodialysis due to renal failure. The structural analysis of these aggregates revealed that full-length wt β2m was the main component of the fibrils[81], together with a truncated form, lacking the first six amino acids at the N-terminus of the protein (ΔN6 β2m), which was constituting the 20-30% of the aggregates. Due to its association with hemodialysis, this condition was named dialysis-related amyloidosis (DRA) [80,81]. The blood analysis of DRA patients revealed an increase up to 60-fold in the concentration of circulating β2m compared to healthy individuals[93]. All this evidence led to the understanding that dialysis was not effective in properly disposing β2m, allowing the protein accumulation in the bloodstream, which eventually underwent amyloid aggregation[94]. Nowadays, thanks to the technological improvement in dialyzers, the incidence of the disease has significantly dropped[56].

Following this pathological association, numerous studies have investigated β2m aggregation process using either *in silico* prediction tools[95–97] or truncated forms of the protein[98,99]. These analyses revealed that about 60% of β2m sequence is potentially amyloidogenic. However, the native structure of the protein is highly resistant to aggregation under physiological conditions[100]. Taken together, this evidence suggests that the predicted β2m aggregation prone regions are largely shielded within its native fold, and that partial unfolding events are required to expose them and initiate fibrillogenesis[101]. Therefore, to study wt β2m fibril formation *in vitro* within a biophysically feasible timescale, a wide range of experimental conditions has been explored. These include the use of cosolvents, as serum amyloid P component – a plasma protein that by binding to pathogens and apoptotic cells, facilitates their clearance from the body –[102], detergents and denaturants, as sodium dodecyl sulphate[103] and trifluoroethanol[104], as well as combinations of low pH (4.5 to 2), and varying

the ionic strength[105–107]. Notably, the morphology of the obtained fibrils change according to the specific conditions applied: fibrils generated at low pH but high ionic strength typically showed flexible and worm-like structures, while those generated at similarly low pH but in absence of ionic strength displayed a long straight structure with a rigid and twisted morphology[107].

However, all these conditions poorly recapitulate the physiological environment in which β_2m aggregation occurs.

To overcome this limitation, a large panel of β_2m mutants has been generated to examine how sequence-specific variations affect the global stability of the protein and, in turn, its aggregation propensity[108,109]. These variants have been deeply characterized through different biophysical and biochemical techniques, and their amyloid aggregation was assessed[93,110–112].

In this framework, considerable attention has been directed towards the region spanning residues 5570, which has been identified by both synthetic peptide analyses and predictive algorithms as the most aggregation-prone segment of the protein[43,95,96,113]. This region, including the loop between strand D and E (DE loop) and the strand E itself, is enriched in aromatic amino acids that participate in non-covalent interactions – particularly hydrogen bonds – establishing with MHC-I heavy chain (Figure 6)[113]. In this thesis project the focus will be on two DE loop mutants, generated by substituting residues Asp59 into Pro and Trp60 into Gly.

The substitution of Asp59 with Pro (D59P) was designed to understand the effect of DE loop stiffening. Its biophysical characterization revealed that the conformational restriction imposed by the Pro markedly reduce overall protein stability and increased aggregation propensity, with amyloid precipitates forming faster and in greater amounts compared to wt β_2m[110].

The role of Trp60 has been extensively explored by replacing it with chemically diverse amino acids, including Phe (W60F)[93], Val (W60V)[114], Cys (W60C)[110] and Gly (W60G)[111]. Substitution with Phe, Val and Cys did not significantly alter β_2m fold stability. However, while W60F readily aggregates, W60V and W60C mutants displayed reduced aggregation propensity[115]. Interestingly, Gly substitution yielded to a more stable and less aggregation-prone protein compared to the other Trp60 mutants[110,111,116]. Taken together, these observations highlight that replacing bulk and hydrophobic moiety, as Trp, with smaller and more polar one, as Gly, increases loop flexibility, thereby enhancing overall protein stability and reducing its aggregation propensity.

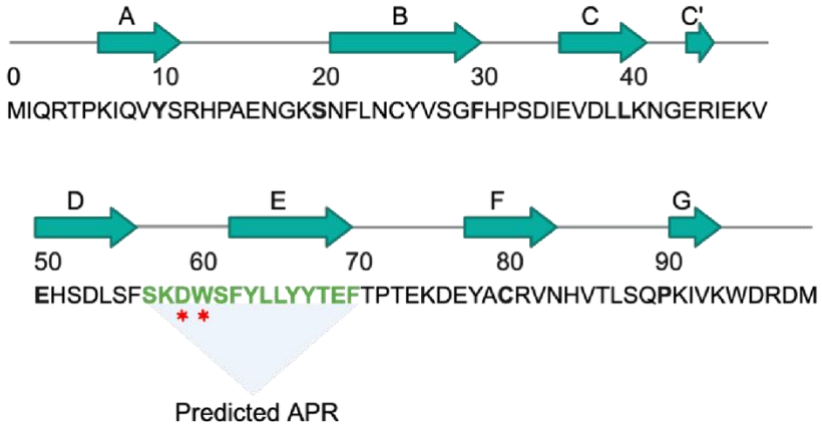

Figure 6: **Amino acid sequence of β_2m**. In green is highlighted the predicted most aggregation-prone region and by red asterisk the residues targeted by the mutations (D59 and W60). Created in https://BioRender.com

In addition to *in silico* designed mutants, in 2012 Valleix *et al.* published a report about the discovery of a natural β_2m variant, in which Asp in position 76 was substituted by an Asn (D76N), causing progressive bowel dysfunction with extended amyloid deposition in the visceral tissues[82]. Differently from DRA, this pathological condition, named hereditary systemic amyloidosis, do not imply increased concentration of circulating β_2m neither kidney involvement. Furthermore, just the fulllength protein was found in the fibrils extracted from patients. The biophysical analysis of D76N indicated that it has lower thermal stability (53.2 °C) compared to the wt protein (62.4 °C) as well as a higher aggregation propensity under physiological conditions.

1.2.1.2 Multiple myeloma

Multiple myeloma (MM) is an incurable hematological cancer characterized by uncontrolled proliferation of plasma cells, causing destructive bone lesions, severe kidney injuries, anemia and hypercalcemia[117]. The average age of onset for the pathology is between 65 to 75 years and it is the third most common hematological malignancy after non-Hodgkin lymphoma and leukemia[118,119]. The primary site of disease is the bone marrow, in which malignant plasma cells accumulate and secrete high levels of monoclonal immunoglobulin proteins, one of the hallmarks for MM. In advanced stages, these malignant cells, also known as circulating plasma cells (CPCs) may also be detected in the peripheral blood, typically indicating a poor outcome for the patients[120,121].

MM progresses through three clinical stages of increased severity and worsening prognosis. These stages are defined by specific biochemical indicators, including serum β2m, albumin and calcium, hemoglobin and lactate dehydrogenase (Table 1)[49].

Table 1: **Prognostic criteria to stage MM from the International Staging System (ISS)**.

Stage	Criteria
I	Serum β2m < 3.5 mg/L Serum albumin ³ 3.5 g/dL
II	Serum β2m < 3.5 mg/L Serum albumin < 3.5 g/dL β2m 3.5 to 5.5 mg/L, independently from serum albumin
III	Serum β2m ≥ 5.5 mg/L

Several clinical studies have demonstrated that the serum concentration of β2m directly correlates with MM tumor burden, defined as the amount of cancer tissue in the body[122,123]. Elevated levels of soluble β2m reflect both the high cellular turnover characteristic of the tumor system as well as the impaired renal function and are strongly associated with poor prognosis and reduced therapeutic response.

For years, the role of β2m in MM was considered purely prognostic. However, in 2021 Hofbauer *et al.* described a novel biological role for β2m, demonstrating that intracellular β2m aggregates induce lysosomal stress and trigger robust NLRP3-mediated inflammation. Their findings revealed that, due to its elevated serum concentration, β2m is phagocytosed by tumor-associated macrophages (TAMs) and internalized by the endo-lysosomal system. Within lysosomes, the combination of low pH (5.04.0) and proteases promotes β2m misfolding and aggregation. Protein fibrils are rigid and highly resistant structures. Therefore, their accumulation over time – in the specific context of β2m in multiple myeloma – progressively induce lysosomal damage, ultimately leading to NLRP3 inflammasome activation[92] (Figure 7).

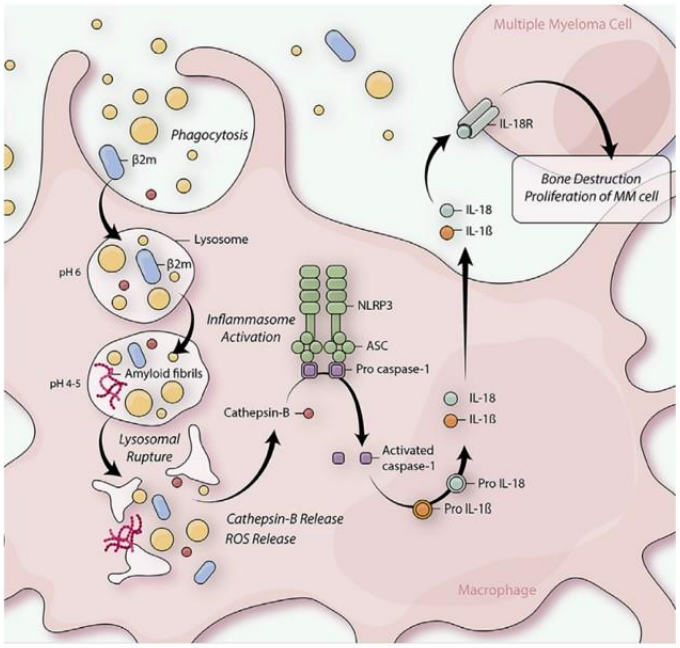

Figure 7: **β_2m phagocytosis by TAMs**. Soluble β_2m is internalized by macrophages and accumulated within lysosomes. Here the lysosomal environment favors the unfolding of β_2m and the formation of amyloid fibrils, which ultimately cause lysosomal rupture and the release of lysosomal content. This rupture triggers the activation of NLRP3 inflammasome and of caspase-1, which cleaves the pro-forms of IL-1β and 18 into their mature forms. These cytokines are secreted by macrophages, fostering a pro-inflammatory milieu that supports the proliferation of myeloma cells. Figure edited from
86.

The NLRP3 inflammasome is a cytosolic multiprotein complex of the innate immune system that regulates the production of mature interleukin-1β and -18. It consists of three subunits a sensor (NLRP3), an adaptor (ASC) and an effector (caspase-1)[124]. The NLRP3 is a tripartite complex formed by a N-terminal pyrin domain (PYD), a central NACHT domain, with ATPase activity essential for NLRP3 self-assembly and proper functionality[125], and a C-terminal leucine-rich repeat domain (LLR domain), which by folding onto the NATCH domain induces inflammasome autoinhibition. The ASC is constituted by a N-terminal PYD domain and a C-terminal caspase recruitment domain (CARD). The caspase-1 has a N-terminal CARD, a central large catalytic domain (p20) and a C-terminal small catalytic subunit (p10)[126].

Inflammasome activation is a tightly regulated process and occurs in two sequential steps. The priming step upregulates the expression of NLRP3, caspase-1 and pro-IL-1β through signaling cascade induced by different pathogen-associated molecular patterns (PAMPs) or damage-associated molecular patterns (DAMPs). These signals are sensed by pattern recognition receptors, such as Toll-like receptors (TLRs), or cytokines receptors, as tumor

necrosis factor (TNF) and IL-1β, leading to the activation of nuclear factor-κB (NF-κB) and the transcription of inflammasome components[124,127]. With the second step the inflammasome is fully activated and assembled in response to diverse stimuli including ATP[128], nigericin[129], bacterial toxins[130], crystalline structures[131] and A-beta fibrils[132] (Figure 8).

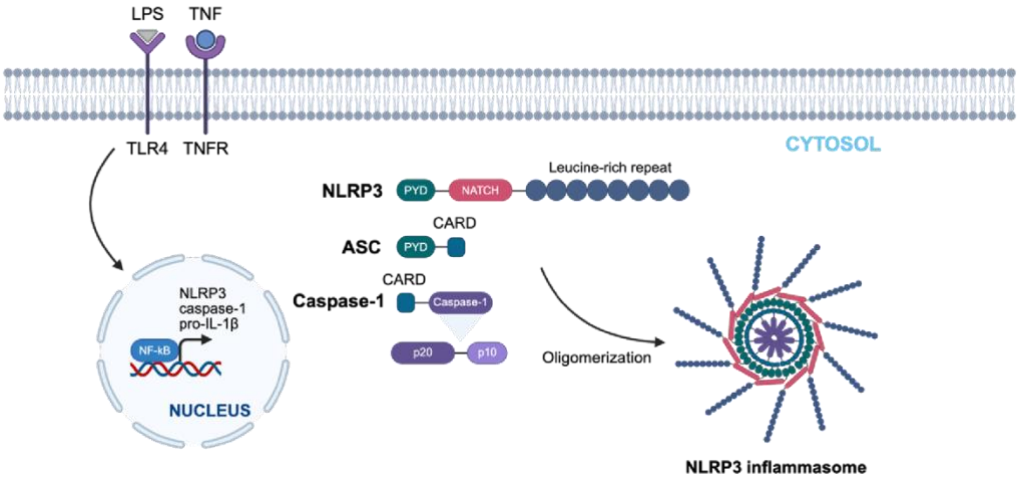

Figure 8: **The NLRP3 inflammasome assembly**. Priming signal recognition activates the NF-κB nuclear factor which initiates the transcription of NLRP3, caspase-1 and pro-IL-1β and the inflammasome oligomerization in the cytosol. Created in https://BioRender.com

NLRP3 inflammasome activation ultimately triggers pyroptosis, a proinflammatory programmed cell death driven by Gasdermin D (GSDMD)[133]. The full length GDSMD is inactive but, upon NLRP3 activation and proteolytic cleavage by caspase-1, its N-terminal fragment oligomerizes and inserts within the plasma membrane, forming large pores, that mediate IL-1β and IL-18 release, eventually causing cell lysis[134].

In this context, Hofbauer *et al.* demonstrated that the activation of the NLRP3 inflammasome results in a huge increase in the secretion of mature IL-1β and -18 by TAMs. Both cytokines are detected in the serum of MM patients and are implicated in MM pathogenesis. IL-1β promotes inflammatory osteolysis – one of the hallmarks of MM –, regulates the migration of plasma cell in the bone marrow, and drives the release of IL-6, which is the central proliferation factor for myeloma cells[135]. Elevated IL-18 concentrations have been associated with poor prognosis[136] and enhanced generation of myeloid derived suppressor cells, which inhibit the T-cell-mediated suppression of MM cells[137]. Furthermore, they showed that β_2m activates TAMs in 5TGM1 mouse model, thus supporting tumor growth and lytic bone lesions. These effects that were significantly reduced treating the mice with MCC950, a selective NLRP3 inhibitor[92].

2. AIM

The aim of my PhD project was to explore the role of β_2m in multiple myeloma.
The lysosomal lumen is a peculiar environment which has been demonstrated to promote β_2m aggregation and, in turn, the activation of NLRP3-driven inflammatory cascade. In this framework, the aim of my thesis is to further dissect the molecular mechanism underlying the pro-inflammatory role of β_2m aggregation in macrophages.

More specifically, the objectives of this work are:

- Assess the effect played by the lysosomal environment on the main biophysical properties of β_2m *in vitro.*
- Investigate whether and how such biophysical properties impact the NLRP3 inflammasome activation and the downstream release of pro-inflammatory cytokines in THP-1 differentiated macrophages.
- Identify which step of β_2m aggregation kinetics is the most critical for triggering the proinflammatory cascade.

To achieve these goals and obtain an extensive characterization of the process, both wild-type and four β_2m variants with unique stability and aggregation propensity were employed: D76N, a naturally occurring β_2m point mutant responsible for hereditary systemic amyloidosis, characterized by lower stability than the wt protein; ΔN6, a truncated form of β_2m lacking the first six N-terminal amino acids, found as major component of *ex vivo* fibrils in amyloidosis patients; D59P, an *in silico*-designed β_2m variant, characterized by enhanced flexibility and high aggregation propensity; W60G, an *in silico*-designed variant with increased structural stability and reduced aggregation propensity relative to wt β_2m.

3. RESULTS

B_2m is a well-known amyloidogenic protein, and its aggregation in the lysosomal lumen of TAMs has recently been associated to the onset of multiple myeloma[92]. However, the molecular mechanisms regulating the entire process, culminating in lysosomal damage and proinflammatory interleukin release, remain poorly understood. In this work, we investigated how lysosomal pH affects β_2m biophysical properties and aggregation propensity *in vitro* and whether the observed effects can disrupt cell physiological functions, ultimately leading to inflammation.

3.1 Impact of pH variation on β_2m biophysical properties

3.1.1 Chemical and thermal stability of β_2m

B_2m wt, D76N, ΔN6, D59P and W60G variants were expressed in *Escherichia coli* and purified by anion-exchange chromatography. To investigate the effect of pH variation on the β_2m fold, we acquired the CD spectra of the β_2m variants at decreasing pH values, ranging from 7.4 to 2.2 (Figure 9). The resulting spectra revealed that β_2m wt completely lost its β-fold features at pH values lower than 4.0 (Figure 9A). In contrast, the W60G variant retained its native assembly even under highly acidic conditions (down to pH 2.2) (Figure 9E). An intermediate behavior was observed for D76N and D59P, which exhibited loss of their native conformation at pH values below 5.0 (Figure 9B and 9D). Notably, ΔN6 spectrum did not show the characteristic features of a β-folded protein and not even an unfolding transition, suggesting that the protein was unfolded at all tested pH values (Figure 9C).

By plotting the CD signal at 202 nm for each β_2m variant across the tested pHs, we determined the pH_m, defined as the pH at which half of the protein is unfolded (Figure 9F). The resulting values, reported in Table 2, closely correlate with the CD unfolding profiles and fall within the pH range typical of the lysosomes (5.0 – 4.5).

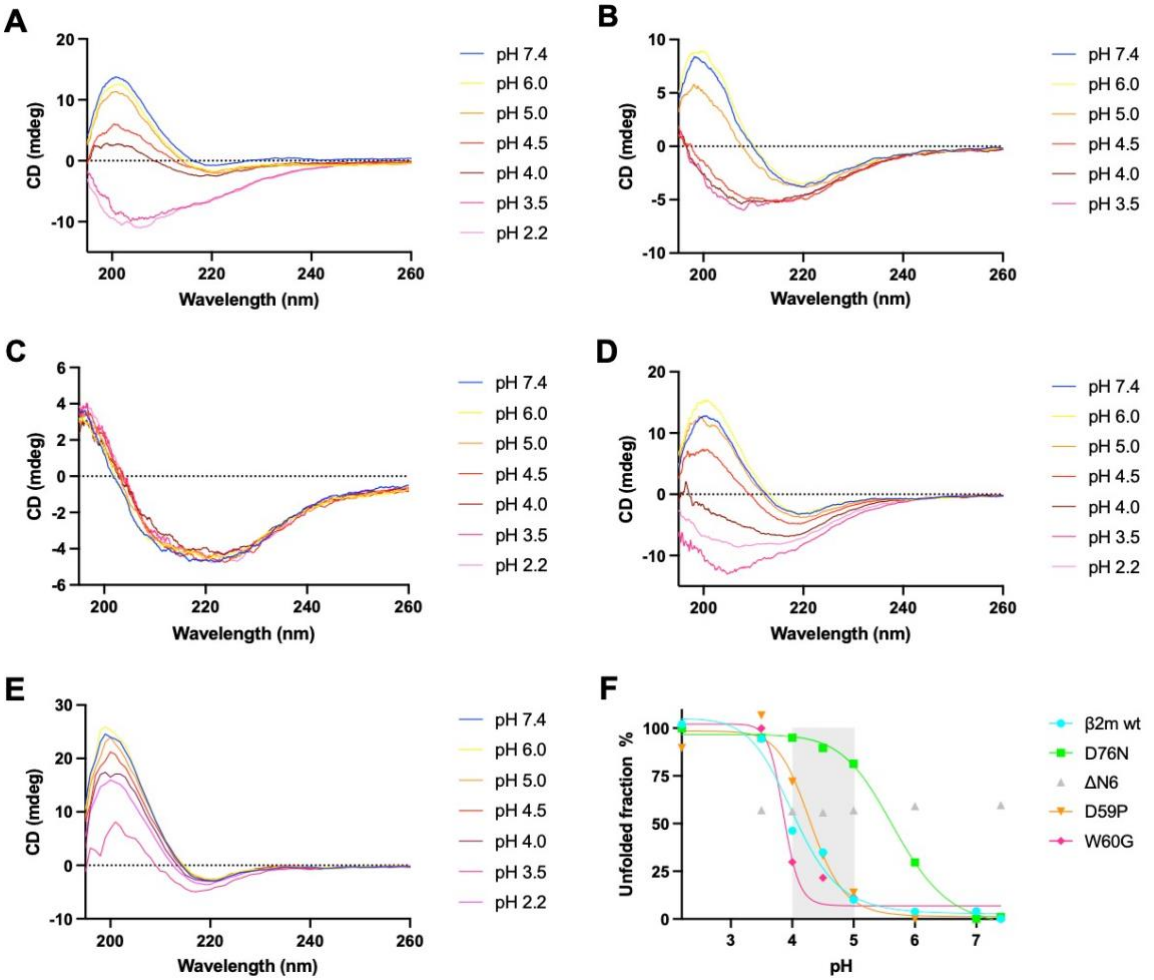

Figure 9: Far-UV spectra of 0.2 mg/mL of β_2m wt (**A**), D76N (**B**), ΔN6 (**C**), D59P (**D**) and W60G (**E**) were recorded at decreasing pH values at 25 °C monitoring the CD signal between 195 and 260 nm. (**F**) pH-dependent denaturation curves obtained by plotting the CD signals at 202 nm for the different β_2m variants at pH variation. The presented spectra derive from the average of three replica.

Additionally, thermal unfolding curves were recorded for each variant at physiological (pH 7.4) and lysosomal-like (pH 4.5) conditions, to assess at which extent the environment acidification influences protein thermal stability. As shown in Figure 10 and summarize in Table 2, the melting temperature (T_m), defined as the first derivative of the thermal unfolding curves, decreased by approximately 15 °C for all the β_2m variants moving from pH 7.4 to 4.5.

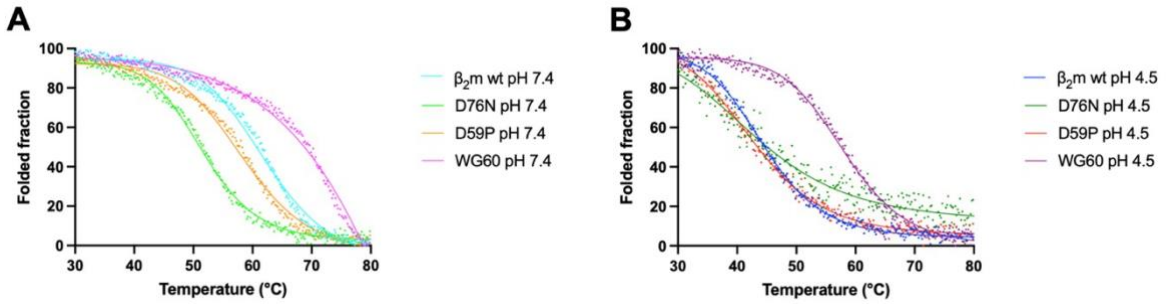

Figure 10: Thermal denaturation for the different β_2m variants at physiological (**A**) and lysosomal-like conditions (**B**) obtained by monitoring the CD signal at 202 nm, increasing the temperature from 30 to 80 °C with a rate of 1 °C/min. The presented spectra derive from the average of three replica.

Table 2: Melting temperature (T_m) and pH melting (pH_m) values, calculated from the thermal unfolding profiles at pH 7.4 and pH 4.5 and the pH-dependent denaturation curve respectively, for the different β_2m variants under analysis (n.d.
= non derivable).

	B_2m wt	**D76N**	**ΔN6**	**D59P**	**W60G**
pH_m	4.03	5.68	n.d.	4.31	3.86
$T_{m\ (pH\ 7.4)}$ °C	62.1	51.6	n.d.	58.5	75.0
$T_{m\ (pH\ 4.5)}$ °C	44.5	43.12	n.d	42.8	58.1

Taken together, these results demonstrated that decrease in pH from 7.4 to 4.0 severely affects the fold of D76N, D59P and β_2m wt. In contrast, W60G is less sensitive to this decrease, retaining its βsheet conformation down to approximatively pH 2.2. The calculated pH_m values fall within the lysosomal pH range (5.0 - 4.0), supporting the observation that β_2m stability is compromised in this cellular compartment. Lastly, the decrease in pH also caused a remarkable drop in protein thermal stability: D59P and D76N were the least thermal stable, followed by the wt, whereas W60G consistently displayed the highest stability. Notably, no biophysical parameters could be determined for ΔN6, as it was already unfolded under physiological conditions. As next step in the biophysical characterization, we investigated the flexibility of the different β_2m variants by means of limited proteolysis under both physiological and lysosomal-like conditions. Indeed, pH variation impact the charge of specific amino acid side chains and therefore the network of interactions that stabilize the protein native fold.

3.1.2 Structural flexibility of β_2m

The effect of lysosomal-like pH on the compactness and flexibility of the different β_2m variants was evaluated by limited proteolysis experiments. Fast proteolytic degradation typically reflects high protein dynamics, whereas slow kinetics are associated with remarkable structural rigidity[138]. To investigate the proteolytic kinetics of the β_2m variants under both physiological and lysosomal-like conditions, two different proteases were used: trypsin and cathepsin B. Trypsin is a serine protease, considered the gold standard for limited proteolysis analysis, and exhibits optimal activity between pH 7.0 and 9.0[139]. In contrast, cathepsin B is a cysteine protease, primarily located inside lysosomes, and possesses optimal activity around pH 4.5 to 5.5[140].

The trypsin proteolytic cleavage was monitored for 240 min with samples retrieved at specific time points as shown in Figure 11. The SDS-PAGE gels revealed distinct proteolytic profiles among the β_2m variants. D76N and ΔN6 displayed comparable proteolytic patterns, with both variants undergoing almost complete degradation within 30 min from the addition of trypsin (Figure 11B and 11C). In contrast, W60G exhibited remarkable resistance to trypsin cleavage: the 50% of cleavage was reached after 180 min of incubation, and notably, 17% of the protein was still uncleaved after 240 min of incubation with the protease (Figure 11E). B_2m wt and D59P showed an intermediate susceptibility to trypsin proteolysis (Figure 11A and 11D). They both reached 50% of cleaved fraction after 60 min incubation with trypsin and were completely digested after 120 min.

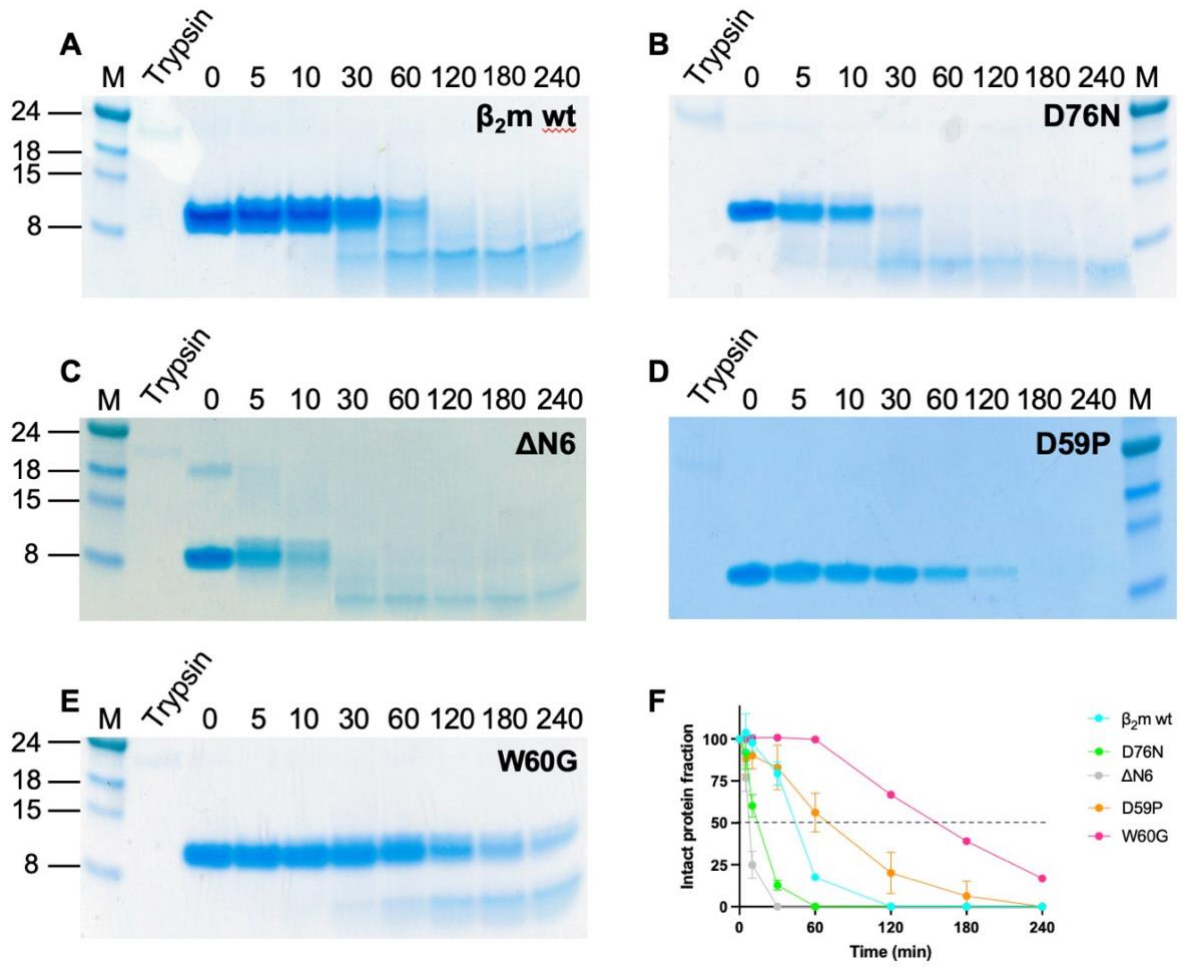

Figure 11: SDS-PAGE gels monitoring limited proteolysis of β_2m wt (**A**), D76N (**B**), ΔN6 (**C**), D59P (**D**) and W60G (**E**) by trypsin. Proteolysis reactions were carried out at a β_2m:trypsin molar ratio of 100:1 in sodium phosphate buffer at pH 7.4 to mimic physiological conditions. Samples were retrieved after 0, 10-,15-, 30-, 60-120-, 180- and 240-min from trypsin addition. (**F**) Kinetics of β_2m proteolysis. Band intensities corresponding to the uncleaved protein fraction were quantified at each timepoint. Data derive from the average of three replica and are expressed as percentage of uncleaved fraction, normalized to the signal at time 0 (100% folded).

Similarly to trypsin, β_2m proteolysis by cathepsin B was followed over 240 min, collecting samples for SDS-PAGE analysis at defined incubation times as shown in Figure 12. Among the tested variants, W60G was the least susceptible to digestion, with over 50% of the protein remaining intact after the full 240-min of incubation (Figure 12E). In contrast, β_2m wt and D59P exhibited the highest sensitivity to the protease treatment, undergoing almost complete proteolysis after 120 min (Figure 12A and 12D). D76N and ΔN6 displayed an intermediate susceptibility; D76N reached 50% cleavage by 60 min whereas ΔN6 after 120 min (Figure 12B and 12C).

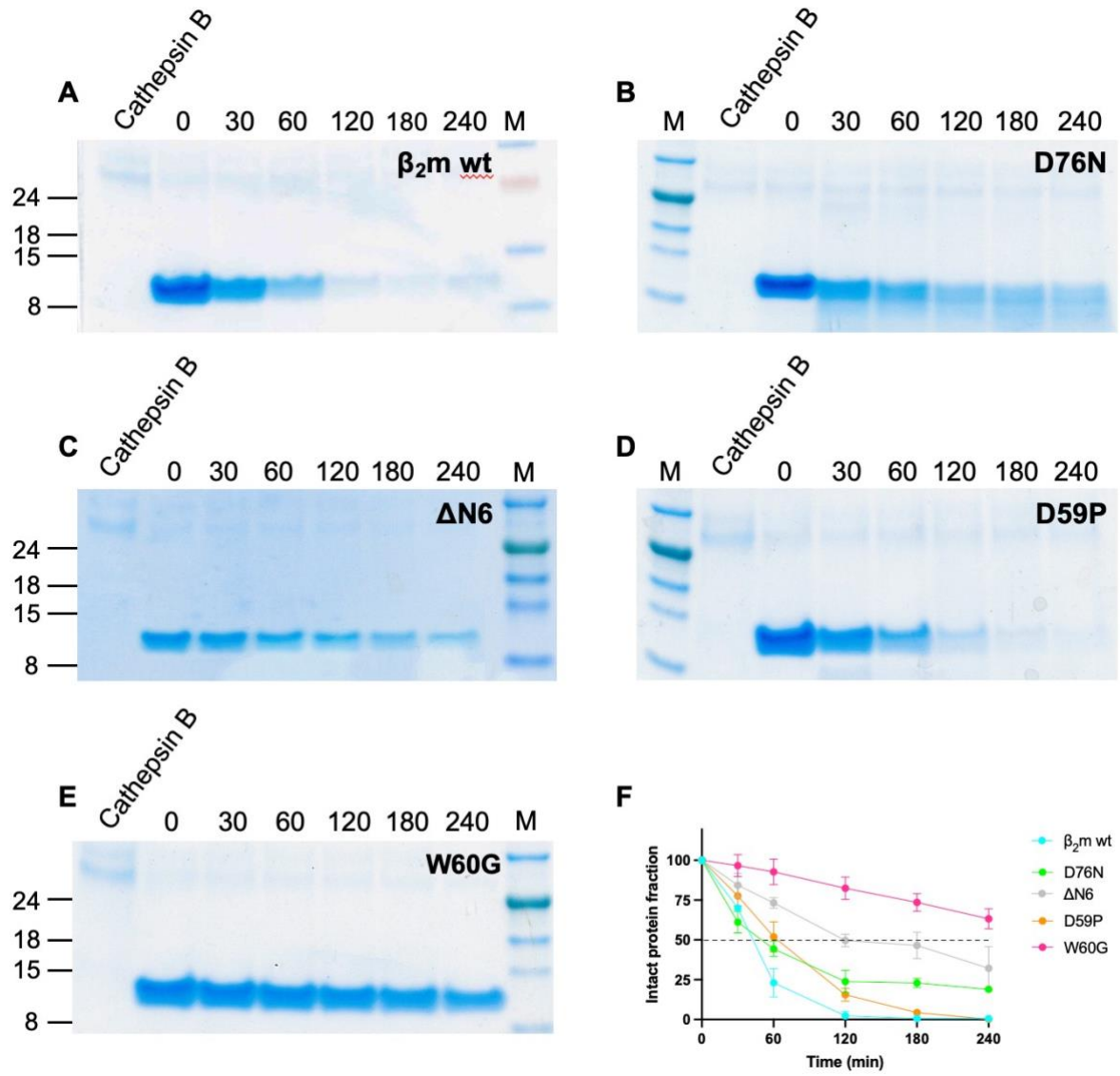

Figure 12: SDS-PAGE gels monitoring limited proteolysis of β_2m wt (**A**), D76N (**B**), ΔN6 (**C**), D59P (**D**) and W60G (**E**) by cathepsin B. Proteolysis reactions were carried out at a β_2m:cathepsin B molar ratio of 25:1 in sodium acetate buffer at pH 4.5 to mimic lysosomal conditions. Samples were retrieved at 0, 30-, 60- 120-, 180- and 240-min after cathepsin B addition. (**F**) Kinetics of β_2m proteolysis. Band intensities corresponding to the uncleaved protein fraction were quantified at each timepoint. Data derive from the average of three replica and are expressed as percentage of uncleaved fraction, normalized to the signal at time 0 (100% folded).

Overall, all the β2m variants underwent almost complete proteolysis after 4 h of incubation with both trypsin and cathepsin B. However, consistently with its higher chemical stability, W60G was less susceptible to proteolytic cleavage and, in the case of cathepsin B, more than 50% of the protein was still uncleaved at the end of the incubation time. Trypsin digestion appears overall harsher than that of cathepsin B, an observation that can be attributes to the higher catalytic efficiency of trypsin.

Based on this proteolytic analysis, we next examined how lysosomal pH influenced the β_2m aggregation tendency, as pH decrease can further modulate the stability and processing of the variants.

3.1.3 B_2m aggregation propensity

Increased flexibility and reduced structural stability are critical factors for aggregation-prone proteins. Indeed, enhanced flexibility often correlates with increased aggregation propensity, especially when hydrophobic regions of the protein become exposed[141]. Therefore, the effect of pH variation – from physiological to lysosomal conditions – on the aggregation propensity of β_2m was evaluated by Thioflavin T (ThT) fluorescence assay. ThT is a fluorescent dye that exhibits strong emission upon binding to β-sheet-rich structures, like the amyloid fibrils. The aggregation kinetics for the different β_2m variants were recorded at pH 7.4 and 4.5, incubating the protein at 37 °C under constant shaking. At physiological pH, none of the β_2m variants underwent aggregation within the experimental timeframe. However, lowering the pH to 4.5 promoted the aggregation for all the variants except for W60G, for which no increase in fluorescence intensity was detected. Particularly, the highest ThT signal was observed for D59P, followed by ΔN6, variants for which the fluorescence increase started after 25 h of incubation. Wt β_2m and D76N curves showed the same profile, characterized by a longer lag phase, with the ThT signal rising after 50 h. ThT positive samples were further investigated at transmission electron microscopy (TEM) to confirm the formation of amyloid aggregates. Negative stain images confirmed the formation of fibrils with distinct morphology depending on the β_2m variant (Figure 13C – F). D76N formed short and stacked fibrils; ΔN6 gave rise to very elongated fibrils; wt and D59P formed fibrils of intermediate length and width.

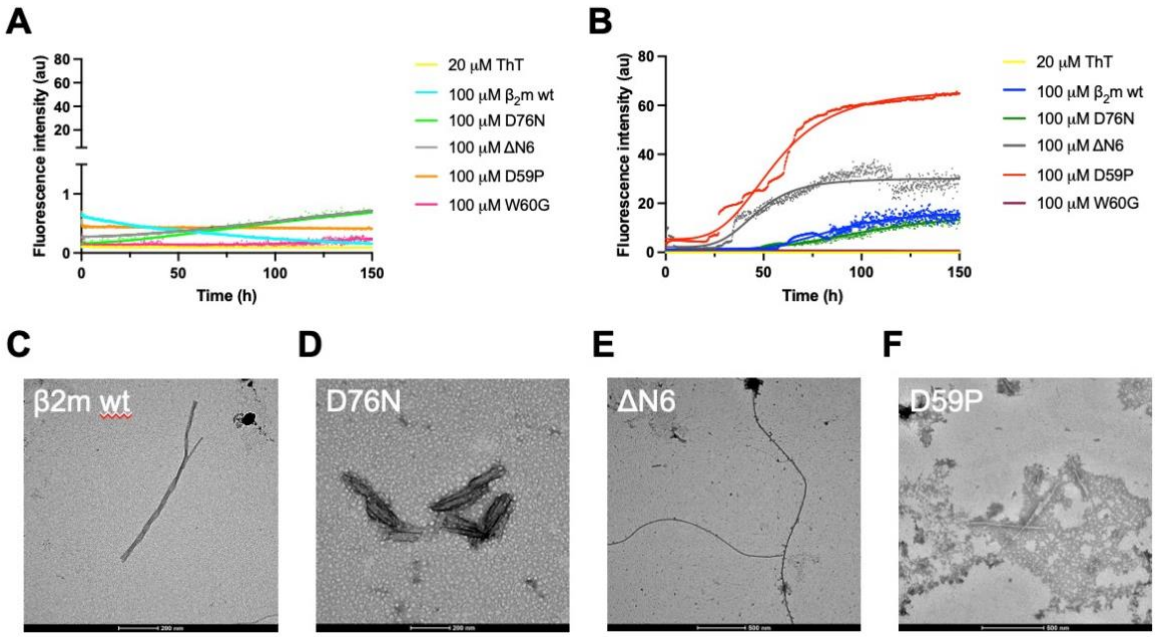

Figure 13: B_2m aggregation was monitored by ThT fluorescence at physiological (**A**) and lysosomal-like conditions (**B**). The aggregation kinetics were recorded for 150 h at 37 °C under agitation. As negative control for fluorescence emission, 20 μM ThT alone was used. The measurements were performed in triplicate. (**C**-**F**) Representative TEM images of negatively stained β_2m fibrils collected from the ThT positive sample – β_2m wt, D76N, ΔN6 and D59P – at pH 4.5.

In summary, the biophysical characterization indicates that lysosomal conditions reduce β_2m stability and increase its flexibility, thereby favoring aggregation. Within this framework, W60G represents an exception, as it remains stable at lysosomal-like pH and consequently does not undergo aggregation. Therefore, to determine whether these biophysical differences translate into distinct cellular responses, we exposed macrophage-like cells to each β_2m variant and evaluated their intracellular accumulation and localization, inflammasome activation and proinflammatory interleukin production.

3.2 B_2m stability affects the strength of NLRP3-mediated inflammation in macrophage-like cells

To understand whether and how the aggregation propensities of the different β2m variants affect the inflammasome activation and the release of pro-inflammatory interleukins, cellular experiments were run using THP-1 cell line.

These cells were isolated from the peripheral blood of a male patient suffering from acute monocytic leukemia and can be differentiated to a macrophage-like state by incubation with phorbol-12myristate-13-acetate (PMA). THP-1 are a widely recognized model for primary macrophages as they possess similar physiology in terms of phagocytosis, cytokines secretion and lipid uptake[142].

In their seminal work Hofbauer *et al.*[92] demonstrated that β2m phagocytosis, and particularly the formation of β2m amyloid aggregates inside the lysosomes, ultimately activate the NLRP3 inflammasome. However, the canonical NLRP3 inflammasome activation pathway, which is at the base of the interleukin-1 maturation and release, requires two signals: the priming step and the assembly step. In our case, we decided to use as inflammation stimulus for the priming step lipopolysaccharide (LPS), which, by binding to its receptor, the Toll-like receptor 4 (TLR4), leads to the upregulation of NLRP3 expression and the transcription of pro-IL-1β through NF-κB pathway[143].

3.2.1 Effect of β2m on cell viability

To assess the effect of β2m wt, D76N, ΔN6, D59P and W60G on cell viability, THP-1-differentiated macrophages, primed with 1 μg/mL LPS, were treated with 30 μg/mL of each mutant and their cellular viability was measured at defined time points using the MTT assay (Figure 14).

The results indicated that all the β2m variants did not exert detectable cytotoxicity during the first 48 h of incubation. However, differences between the treatments became evident at 72 h incubation, with W60G-treated cells displaying the highest viability, whereas D59P mutant induced the most pronounced cytotoxic effect. At later time points (96 and 120 h), the overall cell viability fell below 50% across all conditions, and the differential effect induced by the β2m variants was no longer evident.

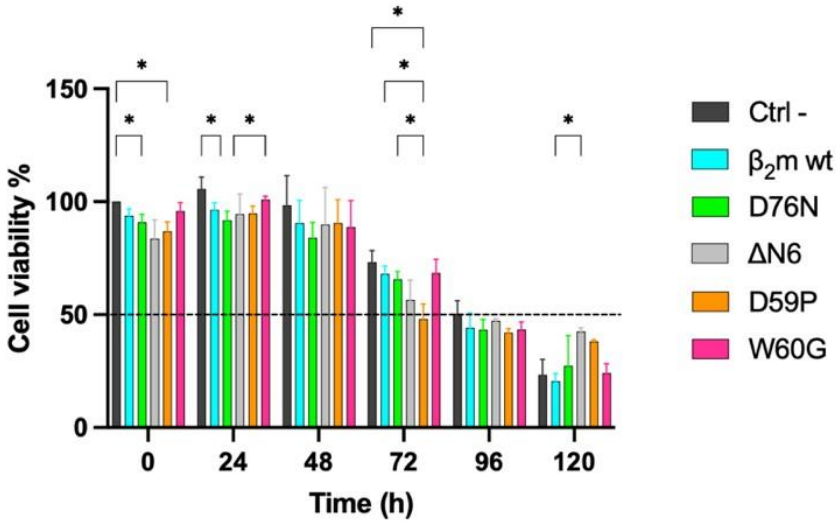

Figure 14: Effect of the treatment with the different β_2m variants on THP-1 viability. Cells were incubated with 30 µg/mL of protein, and their metabolic activity was assessed at 0-, 24-, 48-, 72-, 96- and 120-hours post-treatment by MTT assay. Experiments were performed in triplicate. Data are presented as mean ± SD and expressed as percentage relative to the negative control at time 0, which was set to 100% viability (p= 0.05, mixed-effects analysis).

Since the proteins did not elicit substantial cytotoxicity at the selected concentration until 72 h, we next evaluated the ability of THP-1 cells to phagocytose the different β_2m variants by means of confocal imaging.

3.2.2 B_2m phagocytosis

THP-1 are intrinsically phagocytic cells, and their activity is further enhanced upon differentiation into macrophages. Hence, after seeding, THP-1 were differentiated and primed with 100 ng/mL PMA and 1 µg/mL LPS, respectively. The β_2m variants were labelled with pHrodo green^{TM} STP ester, a pH sensitive dye that strongly emits in acidic environments – such as lysosomes – and added to cells at a concentration of 30 µg/mL. The β_2m cellular uptake was monitored by live-cell imaging. Figure 15 reports the preliminary results on the trend of fluorescent area over time. All the β_2m variants were efficiently phagocytosed by THP-1. However, differences can be detected in the curve shapes depending on the β_2m variant. Indeed, while for wt, D76N and ΔN6 profiles increased linearly overtime, reaching a signal plateau around 24 h of incubation, for W60Gthe fluorescent signal begins to decrease after 60 h. D59P

curve displayed the most significant difference, reaching maximal fluorescence after 12 h of incubation and subsequently decreasing by one-third over the following 60 h.

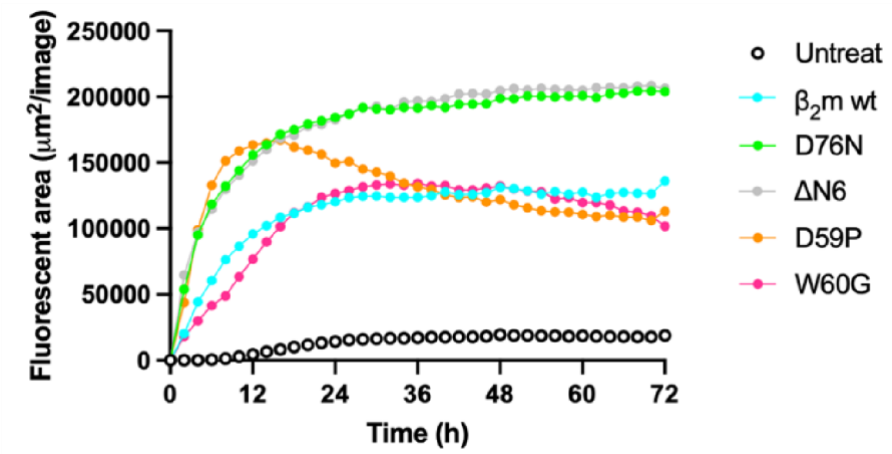

Figure 15: Preliminary data on the trend of fluorescent area detected for differentiated THP-1 after the addition of 30 μg/mL of the different β_2m variants. The proteins were previously stained with pHrodo green ester. The trend of the fluorescent area in each well was monitored by live-cell imaging, for 72 h collecting images at 533 nm every 2 h. The recorded values were corrected by the degree of labelling, calculated for each protein after the pHrodo staining.

Previous evidence suggests that phagocytosed β_2m accumulates within lysosomes, where the acidic environment promotes its aggregation[92]. To investigate how such intracellular accumulation occurred under our experimental conditions, we performed confocal microscopy experiments fluorescently labelling both lysosomes and β_2m.

3.2.3 B_2m intracellular accumulation and localization

To investigate β_2m accumulation kinetics and intracellular localization, confocal microscopy was performed, acquiring images every 24 h for a total of 120 h.

PMA differentiated cells were primed with LPS and treated with 30 μg/mL of the different β_2m variants. After cell fixation and permeabilization, internalized β_2m was labelled using an anti-β_2m primary antibody followed by an Alexa Fluor 488 (AF-488)-conjugated secondary antibody, whereas lysosomes were labelled with LysoTracker Deep Red, a cell-permeable red fluorescent dye that specifically stains acidic organelles.

Figure 16 reports representative results collected for β_2m wt-treated cells. THP-1 at time 0 were included in the analysis to assess the endogenous levels of β_2m and lysosomes prior to the treatment (Figure 16A). After 24 h of incubation, the mean intensity of AF488 and LysoTracker increased, indicating that cells were actively phagocytosing β_2m (Figure 16B). At 48 h, the fluorescence intensity for both the markers decreased (Figure 16C), suggesting that the cells responded to protein accumulation stress by initiating its degradation. By 72 h, the trends of the two signals diverged: β_2m green fluorescence began to rise again, while lysosome red intensity continued to decrease (Figure 16D). This evidence suggests that sustained exposure to high concentration of β_2m drives persistent uptake of the protein and severe intracellular accumulation that ultimately hinders the cell's ability to clear it efficiently. At 96 h of incubation, AF488 intensity further increased before declining again at 120 h. Interestingly, LysoTracker fluorescence followed a distinct pattern. After a linear decrease from 24 to 72 h incubation with the protein, its intensity significantly raised, reaching the maximum at 96 h (Figure 16E), before dropping markedly at 120 h, similarly to β_2m (Figure 16F).

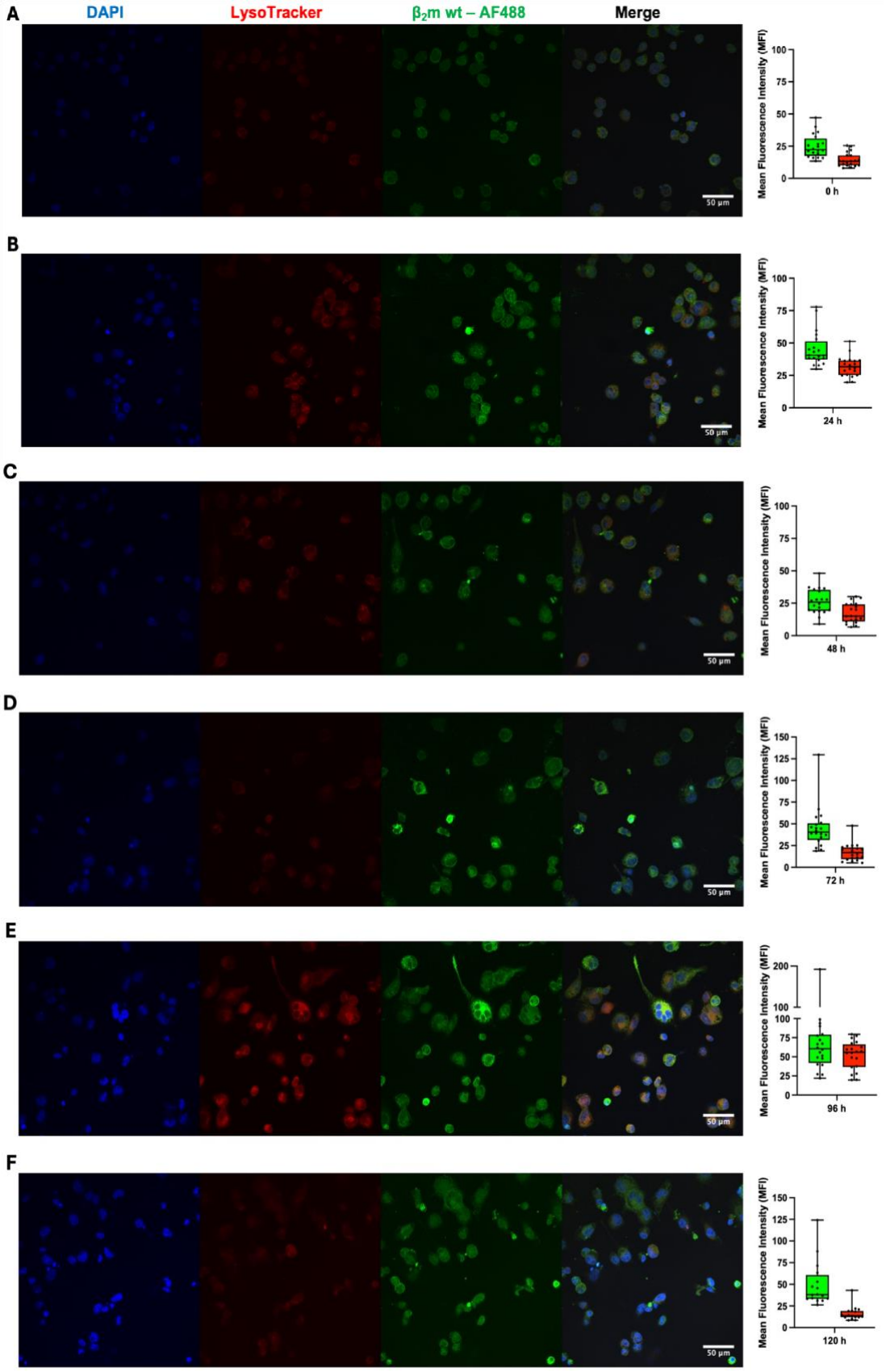

Figure 16: Confocal microscopy images collected for THP-1 cells after 0, 24, 48, 72, 96 and 120 h of incubation with β_2m wt (**A**-**F**). In blue are nuclei stained with DAPI, in red the lysosomes stained with LysoTracker and in

green β2m wt. For each image 20 cells (n=20) were manually picked to calculate the AF488 and LysoTracker fluorescence intensity, represented in the graph as boxplots.

Images collected for cells treated with D76N (Figure 17) revealed AF488 and LysoTracker fluorescence trends consistent with those observed for β_2m wt at the corresponding timepoints. After 24 h of incubation, both AF448 and Lysotracker signals reached their maximum average intensity (Figure 17A). From 48 h onwards, the fluorescence progressively decreased and reached its minimum after 120 h (Figure 17B-E). Interestingly, bright AF488-positive foci appeared starting from 72 h incubation, characterized by a markedly higher intensity than the detected average AF488 fluorescence (17C-E).

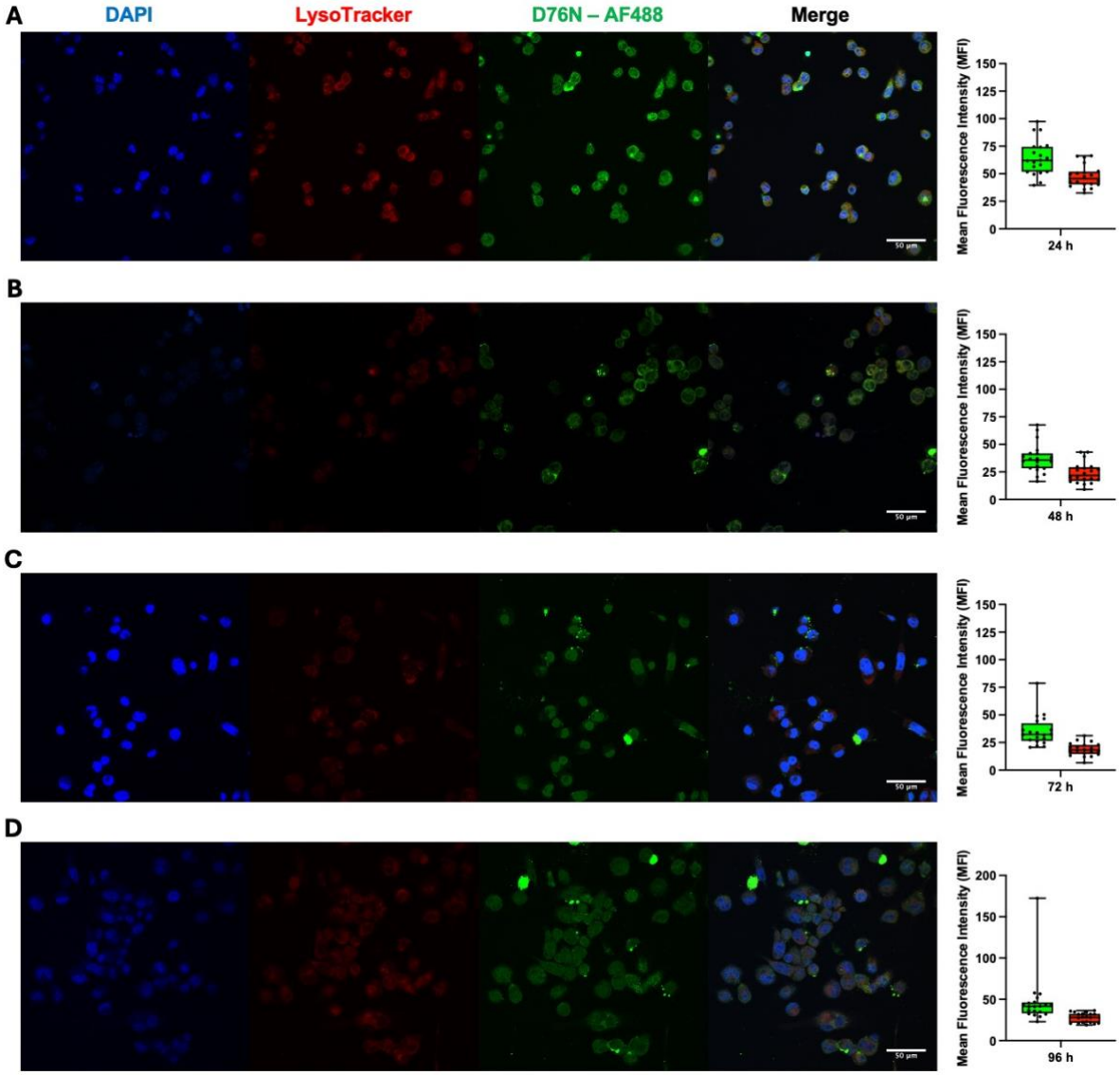

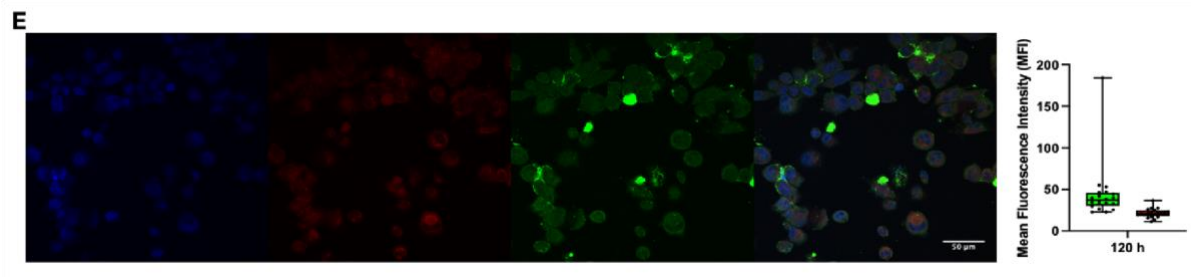

Figure 17: Confocal microscopy images collected for THP-1 cells after 24, 48, 72, 96 and 120 h of incubation with D76N (**A**-**E**). In blue are nuclei stained with DAPI, in red the lysosomes stained with LysoTracker and in green β2m wt. For each image 20 cells (n=20) were manually picked to calculate the AF488 and LysoTracker fluorescence intensity, represented in the graph as boxplots. The arrows indicate the β_2m high fluorescence foci.

Differently from β_2m wt and D76N, the AF488 signal for W60G-treated cells remained consistently low throughout the entire experimental timeframe, with only few highly fluorescent foci detected at long incubation times (Figure 18A-E). These findings suggest that W60G is efficiently degraded by cells, preventing its accumulation and therefore its aggregation.

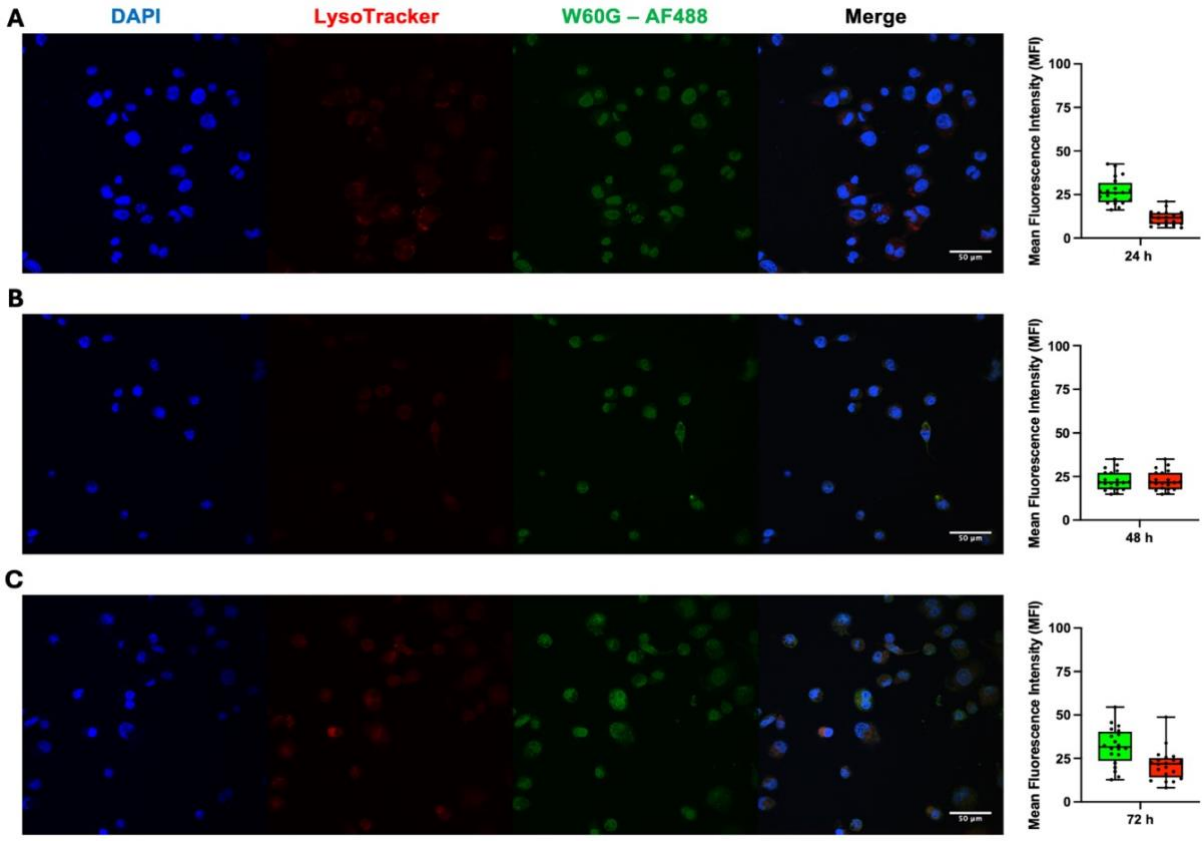

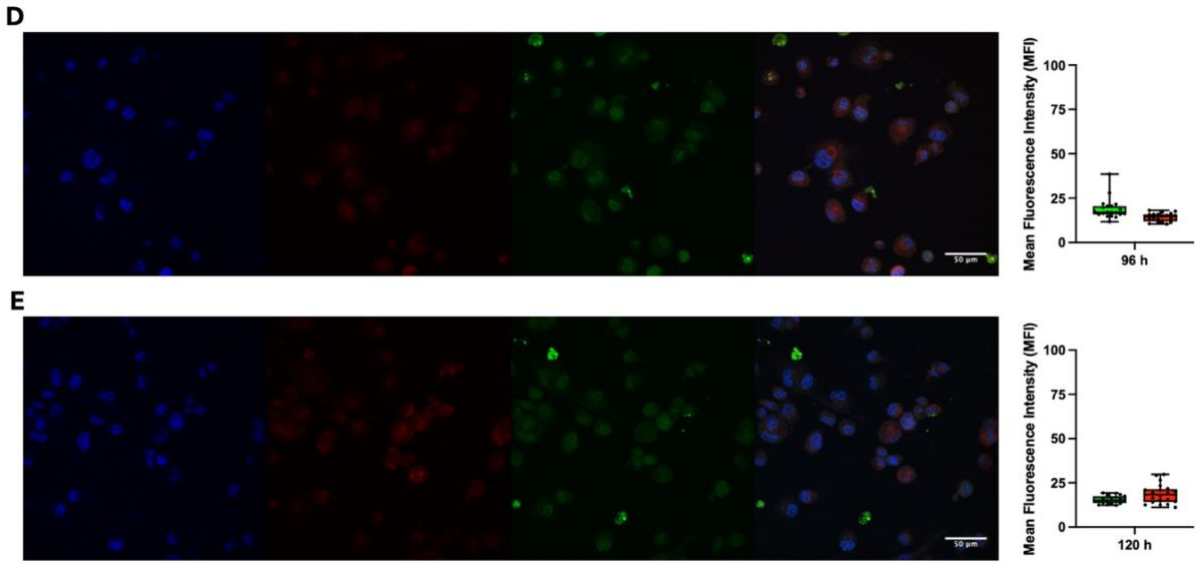

Figure 18: Confocal microscopy images collected for THP-1 cells after 24, 48, 72, 96 and 120 h of incubation with W60G (**A**-**E**). In blue are nuclei stained with DAPI, in red the lysosomes stained with LysoTracker and in green β2m wt. For each image 20 cells (n=20) were manually picked to calculate the AF488 and LysoTracker fluorescence intensity, represented in the graph as boxplots.

These trends are summarized in Figure 19. After 24 h of incubation with β_2m wt and D76N, single cells with markedly elevated AF488 fluorescence were observed, which significantly deviated from the average intensity. This finding suggests that a subset of cells accumulates β_2m to levels that compromise their ability to efficiently degrade it. Conversely, this was not observed for W60G-treated cells, suggesting that cells were able to effectively dispose this variant and therefore it did not accumulate.

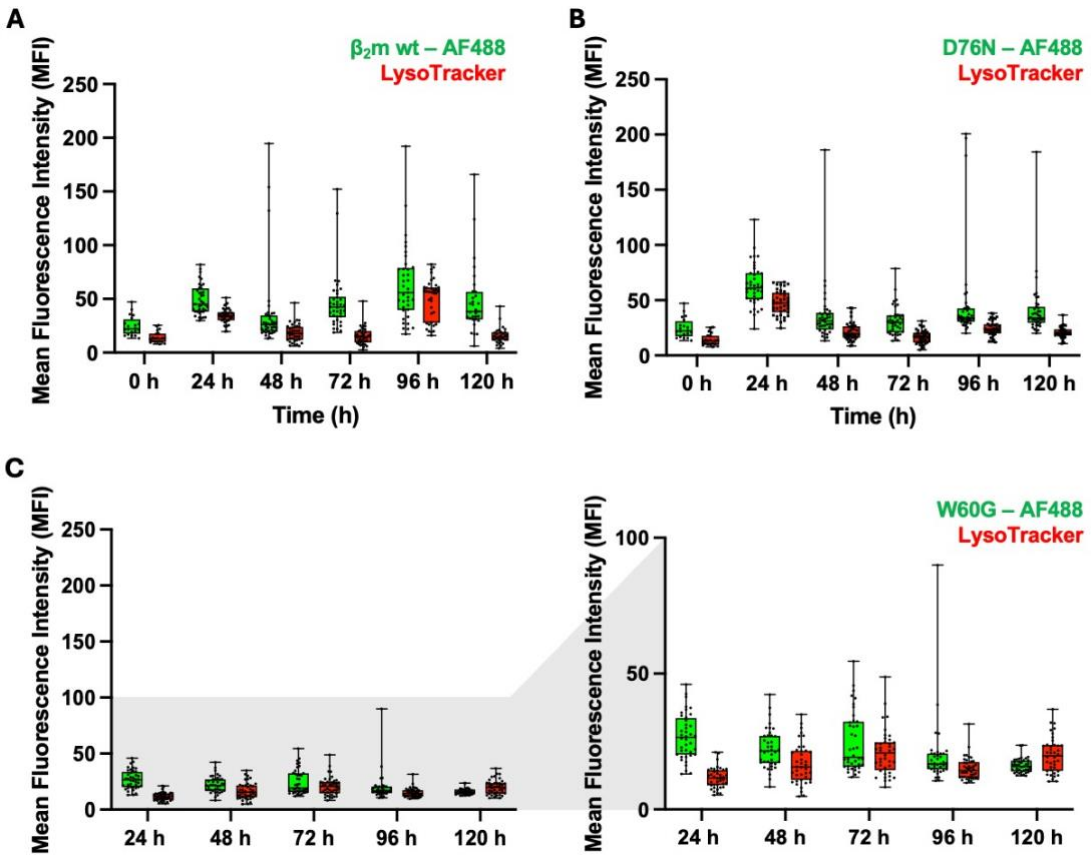

Figure 19: Trend of the β2m-AF488 (green) and lysosome-LysoTracker fluorescence (red) overtime. Boxplot graphs reporting the fluorescence intensities for cells treated with (**A**) wt β2m, (**B**) D76N and (**C**) W60G collected from two different images at each time point (n=40).

Next, to assess the effect of β2m intralysosomal accumulation and determine whether the lysosomal damage – observed in terms of red fluorescence reduction – induce NLRP3 inflammasome activation, we performed western blot analysis.

3.2.4 Inflammatory cascade activation

We next evaluated the ability of the different β2m variants to activate the NLRP3 inflammasomemediated inflammatory cascade. Following PMA differentiation and LPS priming, THP-1 were treated with 30 μg/mL of each β2m variant. Cell lysates were collected after 0, 6, 24, 48 and 72 h of incubation and analyzed by western blot to evaluate the expression of key markers involved in the pathway (Figure 20). These included: NLRP3, the cytosolic multiprotein complex initiating the inflammatory cascade; caspase-1, a key inflammation-mediated caspase activated downstream of inflammasome assembly and essential for the maturation of pro-IL-1β and pro-IL-18; LAMP1, a lysosomal membrane glycoprotein, whose

levels correlate with intracellular lysosomal abundance; β_2m, to assess the amount of protein phagocytosed by the cells; and GAPDH, a constitutively expressed glycolytic enzyme, here used as housekeeping protein for the relative quantification of the markers named above. Negative control samples consisted of macrophage-differentiated THP-1 just primed with LPS, while positive control was obtained by treating LPS-primed cells with nigericin, a microbial toxin that robustly activates the NLRP3 inflammasome by triggering potassium efflux across the cell membrane[144].

The results, summarized in Figure 20, showed that NLRP3 upregulation was activated under all the tested conditions. In negative control cells, peak for inflammasome expression was observed between 24 and 48 h after the LPS priming (Figure 20A), while in nigericin-treated cells, activation occurred earlier, between 0 and 24 h (Figure 20B), confirming the ability of nigericin in triggering the inflammasome assembly.

Interestingly, both the kinetics and duration of NLRP3 activation varied depending on the specific β_2m variant (Figure 20C – 20G). In β_2m wt-treated cells, maximal expression was observed between 6 and 24 h, after which the signal was almost completely lost (Figure 20C). Differently, D76N treatment induced a more stable and prolonged response, that spanned from 6 to 48 h incubation with the protein and declined at 72 h (Figure 20D). ΔN6 triggered an earlier NLRP3 activation, detectable between 0 and 6 h; the signal rapidly decreased thereafter, completely disappearing at 48 h (Figure 20E). D59P induced an effect similar to β_2m wt, with maximal expression between 6 and 24 h incubation, followed by marked decline up to 72 h (Figure 20F). Lastly, W60G treatment led to a delayed NLRP3 response, showing a peak after 24 h incubation (Figure 20G).

Since full inflammasome assembly requires downstream activation of caspase-1, we next evaluated its expression. LPS pre-treatment alone did not induce caspase-1 activation, as shown in Figure 20A, while the addition of nigericin triggered robust overexpression between 6 and 48 h after the compound addition (Figure 20B). In β_2m wt-treated cells, caspase-1 upregulation started after 24 h and declined at 72 h (Figure 20C). D76N addition induced a steady increase, which began after 6 h and persisted up to 72 h incubation with the protein (Figure 20D). ΔN6 treatment induced the strongest caspase-1 response which, similarly to the wt, peaked at 48 h and decreased from 72 h (Figure 20E). Cells treated with D59P displayed an overall weaker activation, that reached its maximum after 48 h incubation (Figure 20F). Remarkably, in W60G-treated cells, caspase-1 expression did not trace NLRP3 activation; indeed, the caspase signal was completely lost after 48 h incubation with the variant (Figure 20G).

Then, we evaluated the effect of β_2m treatment on lysosomal abundance relying on LAMP1 marker. Regardless of the specific variant, β_2m treated cells displayed increased LAMP1 levels compared to both negative and positive control (Figure 20A). However, two distinct patterns emerged: in β_2m wt- and D59P-treated cells, LAMP1 levels fluctuated over time (Figure 20C and 20F), whereas in D76N, ΔN6- and W60G-treated cells, it increased linearly with incubation, ultimately reaching a plateau (Figure 20D, 20E and 20G). Finally, intracellular levels of β_2m were evaluated. While no bands were detected in either the negative or positive controls (Figure 20A and 20B), all β_2m-treated samples displayed clear ones, indicating that the signal is completely dependent on the treatment (Figure 20C – G).

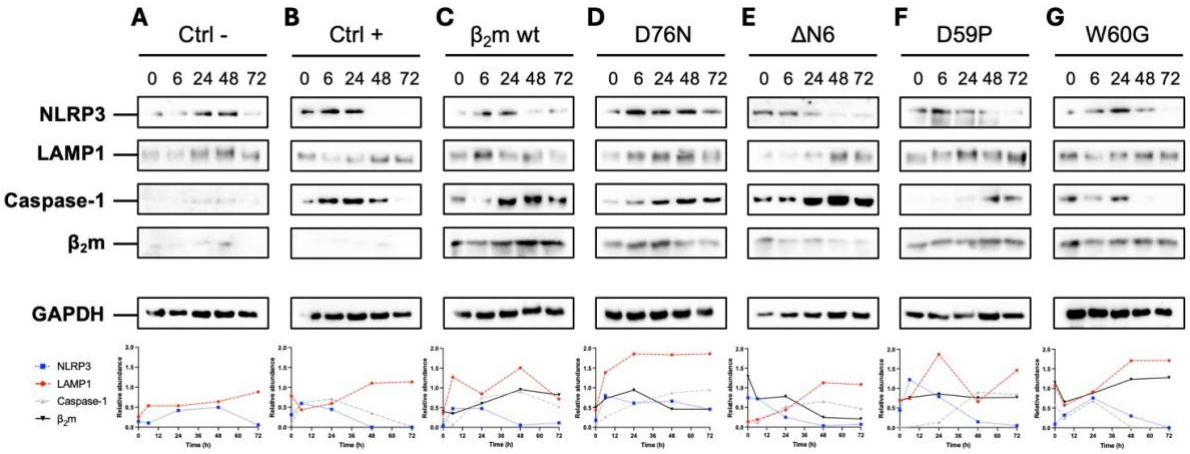

Figure 20: Western blot analysis of total cell lysates to detect NLRP3, LAMP1, caspase-1 and β_2m in LPS-primed THP1-differentiated macrophages. Samples were collected at 0, 6, 24, 48 and 72 hours after the addition of the different β_2m variants (**C**-**G**). Negative control is cells just primed with LPS (**A**), while cells treated with 2 μM nigericin for 1 h were used as positive control for NLRP3 activation (**B**). The protein signal was quantified normalizing the band intensity of each marker by the intensity of GAPDH (NLRP3: 118 kDa; LAMP1: 100 kDa; Caspase-1: 45 kDa; β_2m: 12 kDa; GAPDH: 36 kDa). Two independent experiments were run, and the presented images are representative of the overall cellular behavior.

In summary, all the different β_2m mutants activated NLRP3, but with distinct kinetics. B$_2$m wt and W60G induced activation between 6 and 24 h, which decreased significantly at 48 h; D76N leads to prolonged activation lasting up to 72 h, while ΔN6 and D59P-treated cells displayed earlier activation, with maximum between 0 and 24 h. Inflammasome activation was followed by caspase-1

overexpression for almost all the β_2m treatments, except for W60G-treated cells, where caspase levels declined sharply after 24 h. Variant-specific differences were also observed for LAMP1: wt- and D59P-treated cells displayed fluctuating levels over time, while D76N-, ΔN6- and W60G-treated cells showed a steady increase.

Finally, since NLRP3 inflammasome is the upstream effector responsible for the release of mature IL-1β, we quantified the amount of this cytokine released after cell treatment with each β_2m variant.

3.2.5 Interleukin quantification

The activation of the NLRP3 inflammasome and caspase-1 ultimately leads to the maturation of proIL-1β into its active form. Hofbauer *et al.* demonstrated that its secretion by TAMs sustains the multiple myeloma inflammatory state inducing bone destruction and enhanced proliferation of malignant cells[92]. To assess the impact of the distinct biophysical properties on IL-1β release, differentiated THP-1 cells were treated with 30 μg/mL of each β_2m variant, and supernatants were retrieved after 0, 6, 24, 48 and 72 h incubation. Similarly to western blot, we used as negative control the supernatant of only LPS-pre-treated, whereas as positive control the medium of nigericin-treated THP-1[144].

The levels of IL-1β were quantified by ELISA (Figure 21). The results revealed that β_2m treatment increased the levels of released IL-1β compared to the negative control. Furthermore, for all the tested variants, the cytokine concentrations increased as function of protein incubation time, reaching the release maximum at 72 h. Treatment with D76N resulted in the highest IL-1β release, which reached approximately 150 pg/mL. In contrast, W60G induced the lowest response: IL-1β levels remained consistently lower than those measured for β_2m wt, ΔN6 and D59P at all incubation times, with a maximum of about 50 pg/mL. B$_2$m wt-, ΔN6- and D59P-treated cells displayed intermediate release profile, each reaching a maximal concentration of ~100 pg/mL.

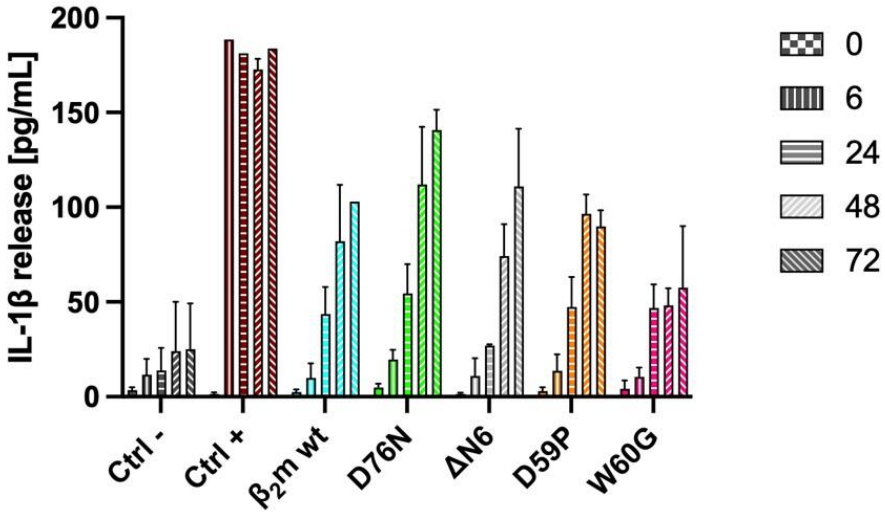

Figure 21: Levels of interleukin-1β (pg/mL) released by THP-1 cells after 0-, 6-, 24-, 48- and 72h incubation with β_2m wt, D76N, ΔN6, D59P and W60G. The negative control corresponds to cells primed with 1 μg/mL of LPS, while the positive control is cells treated with 2 μM nigericin for 1h. Experiments were performed in triplicate and data are presented as mean ± SD.

4. DISCUSSION

Since the 1980s, β2m has been the focus of extensive investigation, following the observation that in patients undergoing long-term dialysis serum levels of β2m were significantly elevated, up to 60-folds higher than in healthy individuals. Such accumulation was found to trigger β2m aggregation into amyloid fibrils, whose deposition represents the hallmark of dialysis-related amyloidosis[80,81].

Elevated β2m levels have also been reported for pathological contexts not directly associated with protein aggregation, as autoimmune diseases[85–87] and hematological malignancies[88,89], including multiple myeloma, a hematological cancer characterized by uncontrolled proliferation of bone marrow plasma cells. Interestingly, in the context of multiple myeloma, β2m has long been used exclusively as prognostic biomarker, as its circulating concentrations consistently correlate with disease severity and tumor burden. However, in 2021, Hofbauer *et al.* demonstrated that β2m also plays an active role in the progression of multiple myeloma. They showed that circulating β2m can be internalized by tumor-associated macrophages within the bone marrow microenvironment and accumulate inside lysosomes. The lysosomal lumen, characterized by low pH (typically 5.0-4.0) and abundant proteases, provides optimal conditions for β2m destabilization, ultimately driving its aggregation into fibrils. The accumulation of such fibrils induces lysosomal rupture and the release of lysosomal content which, by activating the NLRP3 inflammasome, sustains inflammation and facilitates abnormal B-cell proliferation[92].

Extensive *in vitro* evidence indicates that highly acidic pH promotes β2m aggregation[100,101,145,146]. During phagocytosis, proteins experience progressive environmental acidification, shifting from the physiological pH 7.4 in the serum to approximately pH 4.5-4.0 in fully mature lysosome. However, the lysosomal environment is far more complex than pH alone, as it is enriched in enzymes, including hydrolases and proteases, that collectively contribute to protein destabilization and degradation. Therefore, we performed a comprehensive biophysical and cellular analysis to dissect how the different factors present in the lysosomal milieu influence the propensity of β2m to aggregate, as observed in multiple myeloma TAMs.

To obtain a more complete view of the process, in addition to the wt protein, we included four β2m variants with distinct fold stability and aggregation propensity. Specifically, we examined: D76N, the pathogenic variant responsible for the onset of hereditary systemic amyloidosis, which exhibits reduced structural stability and increased aggregation relative to the wt[82,147];

ΔN6, a truncated form of wt β_2m lacking the first 6 residues at the N-terminus, identified in fibrils extracted from dialysisrelated amyloidosis patient and characterized by low fold stability and enhanced aggregation propensity in solution under physiological conditions[148]; D59P, an *in silico*-designed mutant in which replacement of Asp with Pro rigidifies the loop between strands D and E, thereby reducing protein stability and promoting aggregation[110,111]; W60G, another *in silico*-designed mutant in which, oppositely to D59P, substitution of Trp with Gly increases the DE loop flexibility, conferring the protein greater fold stability and a reduced aggregation propensity[110,111]. These variants were expressed, purified and their chemical and thermal stability assessed across a pH range from physiological to highly acidic conditions (pH 7.4-2.2). All the proteins retained the characteristic βfolded structure down to pH 5.0. Among them, D76N and D59P were the most sensitive to pH reduction, showing loss of fold already at pH 5.0. β_2m wt maintained its native conformation to pH 4.0, while W60G proved the most stable, retaining the features typical for β-folded structures up to pH 2.2. Remarkably, ΔN6 was already unfolded at pH 7.4, highlighting its pronounced fold instability. Therefore, except for W60G, all variants underwent structural destabilization within the lysosomal pH range, supporting the notion that environment acidification favors the partial unfolding of the protein[101]. Partial unfolding is a well-established trigger for protein aggregation[101,105]. The thermal stability analysis confirmed such destabilization, showing a significant decrease of approximatively 15 °C in the melting temperature for all the β_2m variants when shifting from pH 7.4 to 4.5. The impact of pH decrease on protein packing and flexibility was analyzed by limited proteolysis, using two proteases with distinct pH optima: trypsin, one of the gold standards for limited proteolysis experiments and most active at physiological pH, and cathepsin B, a lysosomal protease that exhibits maximal activity between pH 6.0 and 4.0. The results demonstrated that all the variants were significantly proteolyzed by both the proteases, except for W60G, which retained a substantial fraction of uncleaved structure at the end of the experimental time frame. This observation is particularly relevant, as increased protein dynamics is a well-known promoter of aggregation. Moreover, it indicates that β_2m can act as substrate for at least one protease populating the lysosomal lumen, suggesting that proteolysis may contribute to lysosomal aggregation. This possibility is particularly interesting, although not yet directly proven, considering that 20 – 30% of *ex vivo* fibrils extracted from DRA patients consist of truncated β_2m form ΔN6. Additionally, ThT aggregation assay showed that lowering the pH to 4.5 initiated aggregation for all variants prone to self-assembly, while W60G remained properly folded. TEM analysis confirmed the fibrillar nature of the aggregates and revealed that, despite identical environmental conditions,

different mutations promoted the formation of fibrils with distinct morphologies. Based on the biophysical characterization performed, the different β2m variants can be therefore classified into three groups according to their fold stability and aggregation propensity under lysosomal-like conditions: i) ΔN6 and D59P, which are strongly destabilized under pH 4.5 and highly prone to amyloid aggregation; ii) wt and D76N, which display intermediate destabilization and aggregation propensity; and iii) W60G, which remains properly folded even under highly acidic condition and does not aggregate.

However, the *in vitro* system alone cannot recapitulate the complexity of the cellular environment, where an intricate network of cell-to-cell contacts, metabolic processes, and stress factors come into play. Therefore, to more closely examine the role of β2m amyloid aggregation in triggering inflammation, we performed cellular experiments on THP-1 cell line. THP-1 are a monocytic line that, upon differentiation with PMA, efficiently mimic macrophage behavior *in vitro* in terms of phagocytosis, response to pathogens and inflammatory signals and cytokine production[149]. THP-1differentiated macrophages were treated with the different β2m variants at a concentration of 30 μg/mL, consistent with the conditions employed by Hofbauer *et al.*[92] and sufficient to elicit measurable effect in the treated samples.

Differentiated THP-1 were efficient in engulfing β2m, and such phagocytosis did not induce any acute cytotoxic effect on the cells. Confocal microscopy analysis of β2m-treated cells confirmed that the protein accumulates inside lysosomes. Both AF488 and LysoTracker fluorescence, which reflects β2m and lysosome signal respectively, increased progressively from 0 to 24 h, suggesting that cells engulf the proteins added to the medium, consistently with the pHrodo live-cell imaging results. At 48 h, in cells treated with wt and D76N variant a marked decrease in both β2m- and lysosome-associated fluorescence was observed; such decline can be explained by the activation of protein degradation pathways by cells in response to the intracellular stress generated by their accumulation. Interestingly, in wt- and D76N-treated cells, after 72 h from the protein addition, β2m signal started to rise again along with the appearance of highly fluorescent AF488 foci, which suggest the formation of intracellular aggregates. The number and size of these green foci increased over time, eventually spreading throughout the entire cell. This phenomenon can be explained by β2m frustrated phagocytosis driven by its high concentration in the culture medium. In parallel, LysoTracker signal decreased, suggesting that aggregate accumulation compromised lysosomal integrity. Indeed, since LysoTracker emits fluorescence exclusively in acidic environments, only intact and functional lysosomes can be labelled; when lysosomal damage alters the organelle internal pH,

the signal declines markedly, as observed for wt- and D76N- treated cells. Conversely, in cells treated with W60G, very few AF488 foci were detected even at long incubation times, suggesting that remarkable stability of this variant under lysosomal conditions allows cells to efficiently degrade it avoiding intracellular aggregate formation.

Elevated accumulation of β_2m aggregates affects cellular inflammation through NLRP3 inflammasome activation. All the different β_2m variants triggered NLRP3 overexpression, but with distinct kinetics. Cells treated with β_2m wt and W60G showed maximum NLRP3 signal between 6 and 24 h, which decreased significantly after 48 h incubation with the proteins; D76N led to prolonged activation lasting up to 72 h, while ΔN6- and D59P-treated cells displayed earlier activation, with maximum signal between 0 and 24 h. The inflammasome overexpression is associated with activation of its downstream effector, caspase-1, which is responsible for cytokine maturation by proteolytic cleavage. Interestingly, cells treated with aggregation-prone β_2m variants, namely wt, D76N, ΔN6 and D59P, showed pronounced caspase-1 activation that persisted up to 72 h. Differently, W60G variant did not induce significant caspase-1 overexpression within the experimental time frame, further confirming the notion that protein stability within the lysosome plays a crucial role in avoiding cellular inflammatory response. Variant-specific differences were observed for LAMP1 dynamics over time. Wt- and D59P-treated cells displayed fluctuating levels over time, whereas D76N-, ΔN6- and W60G-treated cells showed a steady increase. Interpreting these trends is challenging, particularly when compared to LysoTracker signal from confocal microscopy, as the two markers provide different type of information. LAMP-1 reflects the overall lysosomal abundance inside the cells but does not distinguish between functional and damaged organelles. In contrast, LysoTracker fluorescence is strictly dependent on acidic pH, thereby labelling only intact lysosomes. Taken together, the fluctuating lysosomal signal upon β_2m treatment likely reflects an initial phagocytotic phase, in which the organelles increase in number and size, and a subsequent damage-driven decrease caused aggregate accumulation.

Additionally, NLRP3 inflammasome activation is mediator for pyroptosis, a form of proinflammatory programmed cell death driven by caspase-1-dependent cleavage of Gasdermin D (GSDMD)[133]. The N-terminal fragment oligomerization leads to the formation of large pores in the cell plasma membrane, that eventually lead to cytokines and ion release from the cell[134]. Pyroptotic cells are characterized by distinct morphological features including swelling due to water influx through the pores, membrane blebbing, and DNA fragmentation[134,150]. This evidence further supports our findings on NLRP3 activation, ThT aggregation kinetics and cellular toxicity. Specifically, ΔN6- and D59Ptreated cells displayed

early inflammasome activation, which is then completely lost at 72 h, in contrast to β2m wt and D76N, which showed incremental and sustained activation over time. This trends closely matched ThT aggregation, in which ΔN6 and D59P signal increase after 25 h incubation, whereas β2m wt and D76N exhibited longer lag phase, with probe fluorescence rising after 50 h. These differences in aggregation and inflammasome dynamics were also reflected in cell viability measurement: after 72 h incubation, ΔN6 and D59P induced the strongest cytotoxicity, while β2m wt and D76N exerted a milder effect.

Furthermore, confocal microscopy of β_2m-treated cells revealed a progressive increase in cell size, particularly at 96 and 120 h incubation, one of the peculiar morphological features of pyroptotic cells.

Caspase-1 is also responsible for maturation of pro-IL-1β and pro-IL-18 to their active forms[151]. Their secretion by the pyroptotic cells induces the recruitment of various immune cell populations, including monocytes, NK and T cells, which produce chemokines, inflammatory-mediator factors and adhesion molecules[152]. This cascade amplifies the inflammatory response, ultimately leading to tissue damage. In the context of multiple myeloma, the mature IL-1β and -18 secreted by TAMs sustain bone disruption and malignant plasma cell proliferation[92]. ELISA quantification of IL-1β in THP-1 supernatant confirmed the trends observed by confocal and western blot analysis showing that cell treatment with the aggregation-prone D76N variant induce a slightly higher IL-1β release compared to wt, ΔN6 and D59P which display comparable kinetics. In contrast, the stable W60G variant induced lower interleukin release, reinforcing the conclusion that protein stability under lysosomal conditions is a crucial factor in limiting inflammation and reducing proliferative signaling to plasma cells.

Taken together, the data presented in this thesis highlight that β_2m fold stability under lysosomal-like conditions is a crucial factor in preventing inflammation in macrophage-like cells, reflecting what occurs in multiple myeloma TAMs. The combined biophysical and cellular finding suggests that highly aggregation-prone variants, as D76N, formed intracellular aggregates that significantly increase in size with time, consistent with ThT aggregation kinetics which showed a prolonged primary nucleation and aggregates formation starting after 50 h of incubation. The NLRP3 and caspase-1 activation kinetics were similarly prolonged and resulted in elevated release of inflammatory IL-1β. A comparable, but less pronounced effect was observed for wt β_2m, whose fold stability is partially compromised at lysosomal pH, as shown by chemical unfolding analysis. In this case, the resulting intracellular aggregates were generally smaller and led to lower cytokine release. By contrast, cell treatment with W60G

variant, characterized by pronounced stability and absence of aggregation under lysosomal-like conditions, prevents abundant intracellular aggregate accumulation as well as caspase-1 activation and IL-1β release.

Confocal microscopy analysis of ΔN6- and D59P-treated cells will provide the full picture of the process, allowing complete comparison and correlation of the variants' biophysical features and the fine cellular effects detected.

5. CONCLUSIONS AND FUTURE PERSPECTIVES

In this work, we presented a comprehensive characterization of the molecular mechanisms underlying the pro-inflammatory nature of β_2m aggregation in macrophage-like cells.

Overall, the collected data demonstrate that β_2m fold stability under lysosomal-like conditions is a central determinant of its aggregation propensity and proinflammatory potential in THP-1differentiated macrophages, reflecting mechanisms active in tumor-associated macrophages in multiple myeloma. The biophysical characterization revealed that variants with low lysosomal stability and high aggregation propensity, as D76N, formed large intracellular aggregates, prolonged NLRP3 and caspase-1 activation, and elevated IL-1β release. Wt β_2m showed similar but less pronounced effects, in line with its intermediate stability at lysosomal pH. By contrast, the W60G variant, which remains stably folded and aggregation-resistant under acidic conditions, avoided aggregate accumulation and caspase-1 activation, limiting cytokine release. These findings establish a direct link between the structural stability of β_2m and its ability to modulate macrophage inflammatory responses, supporting the concept that β_2m is not only a biomarker but also an active contributor to multiple myeloma pathology.

Completion of the confocal microscopy analyses for ΔN6- and D59P-treated cells will further refine this model, clarifying how subtle differences in variants' structural stability and aggregation kinetics translate into distinct cellular outcomes.

As future outlook for this project, the proliferative effect of IL-1β on myeloma plasma cells will be tested. Indeed, several evidence demonstrated that IL-1β acts as survival signal on multiple myeloma plasma cells, by stimulating the bone marrow stromal cell production of IL-6, and boosts bone resorption, the process by which osteoclasts break down the bone tissue, releasing minerals[135,153]. To evaluate this effect, plasma cells will be treated with THP-1 conditioned medium after β_2m treatment, and their viability will be assessed overtime.

In parallel, investigating the aggregation process holds strong translational potential, as it can guide the development of molecules to stabilize β_2m and reduce the inflammatory state arising from its aggregation. In this context, Visentin *et al.* recently engineered affinity molecules, called affibodies, to specifically target wt β_2m and demonstrated their ability to prevent its aggregation *in vitro* under lysosomal-like environment[146]. Therefore, we wanted to test the ability of these molecules to act in the more complex cellular environment.

Collectively, this thesis provides new mechanistic insights into β_2m-driven inflammation and highlights protein stability as a potential target for therapeutic strategy development against multiple myeloma.

6. MATERIALS AND METHODS

Protein expression and purification

Recombinant β2m wt, D76N, ΔN6, D59P and W60G were expressed and purified following previously reported protocols[148].

Circular dichroism

Circular dichroism measurements were performed on a J-1500 spectrometer (JASCO Europe), equipped with a Peltier system for temperature control, using quartz cuvette with a 0.1 cm path length. Far-UV spectra were recorded at increasing pH values (2.2, 3.5, 4.0, 4.5, 5.0, 6.0, 7.4) from 195 to 260 nm at 25°C and the chemical unfolding profiles were obtained by deconvolution of these spectra. B_2m variants were diluted to 0.2 mg/ml in 20 mM buffer (Sodium phosphate for pH 7.4, 6.0; Sodium acetate for pH 5.0. 4.5, 4.0, 3.5, 2.2) and incubated at room temperature (RT) for 30 min before each measurement. The pH melting (pH_m) values were calculated as the first derivative of the unfolding profiles. Thermal unfolding was assessed monitoring the CD signal at 202 nm between 30 and 80 °C with a heating rate of 1 °C/min. The melting temperature (T_m) at pH 7.4 and 4.5 was calculated as the first derivative of the unfolding profile. Each measurement was performed in triplicate. The average data were normalized between 0 and 100 and fitted to a sigmoidal function using GraphPad PRISM 10.

Limited proteolysis

B_2m wt, D76N, D59P and W60G were diluted to 0.5 mg/mL in 20 mM Sodium phosphate, 150 mM NaCl, pH 7.4 and were incubated with trypsin (Thermo Fisher Scientific) at 37 °C at a molar ratio of 100:1, respectively. Samples were collected after 0, 15, 30, 45, 60, 120 and 240 min after protease addition, mixed with 4X sample buffer (Invitrogen) and heated at 95 °C for 10 min. Denatured samples were analyzed on 12% SDS-PAGE gel. For digestions with cathepsin B (Thermo Fisher Scientific) β2m wt, D76N, ΔN6, D59P and W60G were diluted to 0.5 mg/ml in 20 mM Sodium acetate, 150 mM NaCl, 30 mM DTT, pH 4.5. The protease was added at protein-to-protease molar ratio of 25:1. Prior the digestion started, cathepsin B was pre-activated by dilution in 20 mM Sodium acetate, 15 mM EDTA, 30 mM DTT, pH 5.0 and incubation for 15 min at 25 °C.

The band intensities were quantified using Fiji installation of ImageJ[154] and the fraction of uncleaved protein was plotted as function of incubation time with the protease using GraphPad PRISM 10.

Thioflavin T aggregation assay

B_2m variants were diluted at a final concentration of 100 µM in 20 mM Tris-HCl, pH 7.4, or 20 mM Sodium Acetate, pH 4.5 and supplemented with 20 µM freshly prepared Thioflavin T (ThT). Aliquots of 50 µl of each condition were loaded in triplicate in black, clear-bottom 96-well plates and the ThT signal was recorded for 150 h at 37 °C under mild agitation with an excitation/emission wavelength of 450/480 nm, bottom read and a gain of 1000. The measurements were performed using a Varioskan LUX microplate reader (Thermo Fisher Scientific). Data were analyzed and fitted to a sigmoidal function using GraphPad PRISM 10.

Transmission electron microscopy

At the end of the aggregation kinetics, 10 µl of the samples positive at the ThT was applied onto a 400-mesh copper carbon-coated grid (Agar Scientific) and, after 1 min incubation, the sample excess was removed. The grid was then stained with 2% (w/v) uranyl acetate solution, blotted dry, and imaged on a Talos L120C transmission electron microscope (Thermo Fisher Scientific) operating at 120 kV.

THP-1 cell line

THP-1 monocytic cell line (ATCC) was cultured in suspension in RPMI-1640 medium (Euroclone) supplemented with 10% heat inactivated FBS (Euroclone) and 1% penicillin/streptomycin (Euroclone) at 37 °C with 5% CO_2. Monocyte differentiation into macrophages was achieved treating cells with 100 ng/mL of phorbol-12-myristate-13-acetate (PMA) (Thermo Fisher Scientific) for 24 h, followed by recovery in fresh medium for 24 h.

Cell viability assay

Cell viability after treatment with β_2m wt, D76N, ΔN6, D59P and W60G was assessed by 3-(4,5dimethylthiazol-2-yl)-2,5-diphenyltetrazolium bromide (MTT) assay. Cells were seeded in triplicate at a concentration of 25,000 cells/well in a 96-well plate and, after differentiation and priming with LPS (1 µg/mL for 1 h), they were treated with 30 µg/mL of the different β_2m variants for 0, 24, 48, 72, 96 and 120 h. At the end of the incubation time, MTT assay was performed according to the instructions of the manufacturer (Roche). The absorbance was

recorded at 550 nm (reference wavelength 690) using Varioskan LUX plate reader (Thermo Fisher Scientific). Each experiment was performed in triplicate, and the results were presented as mean of the replicas ± SD. The statistical analysis (two-way ANOVA with multiple comparisons) was performed with GraphPad PRISM 10.

Live cell imaging

THP-1 cells were seeded in triplicate in a 96-well plate at a density of 20,000 cells/well. Following the differentiation, macrophages were primed with 1 μg/mL LPS (Thermo Fisher Scientific) for 1 h. Cells were washed with PBS and treated with 30 μg/mL of β_2m wt, D76N, ΔN6, D59P and W60G previously stained with pHrodo^{TM} iFL Green STP Ester (Thermo Fisher Scientific) according to the manufacturer's instruction. pHrodo fluorescence was recorded for 72 h acquiring the signal at 533 nm every 2 hours with Incucyte S3 (Sartorius) live-cell analysis system at the Advanced Light and Electron Microscopy Imaging Center (ALEMBIC) facility of the I.R.C.C.S. Ospedale San Raffaele. The total fluorescence area was collected and analyzed using the Incucyte Live Cell Image Analysis software. Data were analyzed using GraphPad PRISM 10 software.

Confocal microscopy

THP-1 were seeded in a 8-chambered slide at a density of 75,000 cells/chamber. Following differentiation and LPS priming (1 μg/mL for 1 h), cells were treated with 30 μg/mL of β_2m wt for 0, 24, 48, 72, 96 and 120 h and fixed with 4% formaldehyde for 15 min at RT. After 3 washes with PBS, samples were permeabilized with 0.01% Tween-20 in PBS (Euroclone) for 5 min and washed three times. To block nonspecific binding sites, cells were incubated with 1% bovine serum albumin (BSA) in PBS for 1 h at RT and then stained combining the use of antibodies and fluorescent probes. Particularly, lysosomes were labelled with 100 nM LysoTracker Deep Red (Thermo Fisher Scientific) for 1.30 h at 37 °C with 5% CO_2. B$_2$m was labelled with rabbit anti-β_2m (Cell Signaling Technology) antibody at 1:500 dilution for 1 h at RT. As secondary antibody, a goat anti-rabbit antibody conjugated with Alexa Fluor 488 (Thermo Fisher Scientific) was used at 1:1000 dilution for 1 h at RT. Lastly, cells were mounted with a drop of ProLong Diamond Antifade mountant containing DAPI (Thermo Fisher Scientific) for nuclei staining.

The slides were examined with an ECLIPSE Ti2 inverted microscope (Nikon) at the Unitech NOLIMIT platform of the Università degli Studi di Milano. Images were collected at a magnification of 60X, with the same confocal settings in terms of laser power (12 for DAPI, 5 for AF488, and 3 for LysoTracker Deep Red) and gain (55 for DAPI, 30 for AF488 and 28 for

LysoTracker Deep Red) and pinhole set to 1. Twenty cells were manually selected in each image, and the AF488 (green) and LysoTracker (red) mean fluorescence was quantified using Fiji installation of Image J. To account the background contribution, the background signal of each image was subtracted to the intensity of both the green and red fluorescence.

Western blot

Differentiated THP-1 were seeded in a 12-well plate at a density of 300,000 cells/well, primed with LPS (1 µg/mL for 1 h) and treated with 30 µg/mL of β2m wt, D76N, ΔN6, D59P and W60G. Samples were collected after 0, 6, 24, 48 and 72 h of incubation with the proteins and directly lysed in a fixed volume (150 µL) of 2% SDS lysis buffer (50 mM Tris-HCl pH 7.4, 150 mM NaCl, 5 mM EDTA, 2% SDS) supplemented with cOmplete Protease Inhibitor Cocktail (Roche). Cell debris was removed through centrifugation at 16,000 *x g* for 15 min at 4 °C. Protein extracts were supplemented with 4X Laemmli buffer (62.5 mM Tris-HCl pH 6.8, 2% SDS, 10% glycerol, 5% 2-mercaptoethanol and 0.005% Bromophenol Blue) and denatured for 10 min at 95 °C. An aliquot of 20 µL of proteins were loaded on 12% SDS-PAGE, which was run with 1X MOPS buffer. At the end of the electrophoretic run, the gel was transferred to 0.45 µm nitrocellulose membrane. Membranes were blocked in 5% milk dissolved in TBS-T (20 mM Tris-HCl pH 7.4, 150 mM NaCl, 0.1% Tween-20), and immunodecorated with rabbit primary antibodies directed against NLRP3 inflammasome (Cell Signaling Technology), LAMP1 (Cell Signaling Technology), caspase-1 (Cell Signaling Technology), β2m (Cell Signaling Technology) and GAPDH (Cell Signaling Technology), at 1:2,000 dilution for 16 h at 4 °C. Membranes were then incubated with HRP-conjugated goat anti-rabbit antibody (Thermo Fisher Scientific) at 1:5,000 dilution for 2 h at RT. Protein signals were detected by chemiluminescence using ChemiDoc MP imaging system (Bio-rad). The intensity of the bands was quantified using Fiji installation of ImageJ[154] and subsequently normalized to the corresponding GAPDH band to obtain the relative protein abundance for each marker (NLRP3, LAMP1, caspase-1 and β2m). Data were analyzed using GraphPad PRISM 10 software. Two independent experiments were performed, and the presented images are representative of the overall cellular behavior.

Enzyme-linked immunosorbent assay – ELISA

Similarly to the lysates, cell supernatants were collected after 0, 6, 24, 48 and 72 h incubation with β2m wt, D76N, ΔN6, D59P and W60G and the concentration of interleukin-1β in each sample was determined by ELISA. Each condition was tested in duplicate, as instructed by the

manufacturer (R&D Systems), and three independent experiments were performed. Sample fluorescence was recorded at 450 nm (reference wavelength 540 nm) using Varioskan LUX plate reader (Thermo Fisher Scientific). Data were analyzed using GraphPad PRISM 10 software.

During the preparation of this thesis, the author used GTP-4 to rephrase, improve writing style and check grammar and spelling. After using this tool, the author reviewed and edited the text as needed and take full responsibility for the content of this work.